Finite Feynman integrals

Giulio Gambuti,[1,*] David A. Kosower,[2,3,†] Pavel P. Novichkov,[2,‡] and Lorenzo Tancredi[4,§]

[1]*Rudolf Peierls Centre for Theoretical Physics, University of Oxford, Clarendon Laboratory, Parks Road, Oxford OX1 3PU, United Kingdom*

[2]*Institut de Physique Théorique, CEA, CNRS, Université Paris–Saclay, F–91191 Gif-sur-Yvette cedex, France*

[3]*Theoretical Physics Department, CERN, CH-1211 Geneva, Switzerland*

[4]*Physik Department, Technische Universität München, James-Franck-Straße 1, D–85748 Garching, Germany*

(Received 22 March 2024; accepted 12 September 2024; published 31 December 2024)

We describe an algorithm to organize Feynman integrals in terms of their infrared properties. Our approach builds upon the theory of Landau singularities, which we use to classify all configurations of loop momenta that can give rise to infrared divergences. We then construct bases of numerators for arbitrary Feynman integrals, which cancel all singularities and render the integrals finite. Through the same analysis, one can also classify so-called evanescent and evanescently finite Feynman integrals. These are integrals whose vanishing or finiteness relies on properties of dimensional regularization. To illustrate the use of these integrals, we display how to obtain a simpler form for the leading-color two-loop four-gluon scattering amplitude through the choice of a suitable basis of finite integrals. In particular, when all gluon helicities are equal, we show that with our basis the most complicated double-box integrals do not contribute to the finite remainder of the scattering amplitude.

DOI: 10.1103/PhysRevD.110.116026

I. INTRODUCTION

Feynman integrals are key building blocks for observables in high-energy physics. The integrals contributing to any scattering amplitude satisfy many linear relations. Within dimensional regularization [1,2], integration-by-parts (IBP) identities [3,4] provide these relations systematically. Solving these relations allows us to express scattering amplitudes in terms of a basis of so-called master integrals. As with the basis in any linear space, the choice of master integrals is not unique. Different choices may be appropriate for different purposes. For instance, canonical bases [5–7] are particularly well suited to the computation of the integrals themselves via the method of differential equations [8–11]. However, such bases are not necessarily the best option when seeking a compact representation for scattering amplitudes. The choice of an optimal basis for general multiloop scattering amplitudes is not known; indeed, even the criteria for such a representation are a matter of debate.

In this article we investigate this problem, with Yang-Mills and gravity theories in mind. These theories exhibit both infrared (IR) and ultraviolet (UV) divergences. In dimensional regularization both appear as poles in the regulator ϵ. The IR structure of scattering amplitudes offers a natural path to selecting bases of Feynman integrals. As an example, the authors of Refs. [12,13], following two different approaches, simplified the calculation of the four-loop QCD cusp anomalous dimension. Each chose a basis of master integrals that minimized the number and complexity of IR-divergent integrals required. IR-finite integrals have also been employed [14,15] to simplify the calculation of the mixed QCD-electroweak corrections to the production of a Higgs boson and a jet. These findings support the idea that organizing integrals according to their IR properties has the potential to simplify not only the final form of the result but also the computation of scattering amplitudes.

Leveraging IR factorization [16–21], a possible way of making the IR structure of an L-loop amplitude manifest is to split it into hard and IR-divergent parts, $\mathcal{A}^{(L)} = \mathcal{A}^{(L)}_{\text{hard}} + \mathcal{A}^{(L)}_{\text{IR}}$, where the latter contains all IR divergences of the amplitude. One would then expect that the hard part $\mathcal{A}^{(L)}_{\text{hard}}$ should be described in terms of IR-finite integrals, while the IR part $\mathcal{A}^{(L)}_{\text{IR}}$ in terms of a minimal set of

*Contact author: Giulio.Gambuti@new.ox.ac.uk
†Contact author: David.Kosower@ipht.fr
‡Contact author: Pavel.Novichkov@ipht.fr
§Contact author: Lorenzo.Tancredi@tum.de

(presumably simpler) divergent integrals. However, this decomposition is not unique since $\mathcal{A}_{\mathrm{IR}}^{(L)}$ is only determined up to finite contributions. While offering a complete solution to this problem goes beyond the scope of this paper, a comprehensive understanding of IR-finite Feynman integrals provides a solid starting point to investigate these questions. This sets our immediate goal: in this paper we focus on the algorithmic classification of finite Feynman integrals. These integrals fall into three different classes: *locally finite*, *evanescent*, and *evanescently finite*. We provide a systematic approach to these classes, as well as conjectures for all-loop results.

Locally finite integrals have integrands whose singularities are integrable. They can be computed directly in four dimensions and are in that sense more robustly finite than integrals in the third category. Von Manteuffel *et al.* previously developed [22,23] an approach to constructing bases of finite integrals, which was then generalized in Ref. [24]. Their approach relied on the study of Feynman integrals in parametric representation, where their finiteness can be determined from the degree of divergence in the individual integration parameters. Finite integrals can then be determined by adding powers of the individual propagators and considering them in different numbers of spacetime dimensions. While this approach is strictly guaranteed to work only in the Euclidean case, it has already found application in various state-of-the-art calculations [25–28]. In an entirely different approach, Anastasiou and Sterman have shown how to analyze the IR structure of Feynman integrands [29], and have also shown an application to an amplitude [30]. Others [31–34] have relied on IR properties to organize integrands for complete amplitudes rather than studying Feynman integrals separately.

Finite integrals are simpler to evaluate. It is easier to compute them analytically by direct integration [35]. They also are easier to evaluate to high precision using purely numerical methods either with sector decomposition [27] or methods based on tropical geometry [36].

Evanescent integrals are a subset of locally finite integrals which vanish in four dimensions, but are nontrivial in D dimensions. That is, they evaluate to $\mathcal{O}(\epsilon)$ and therefore do not contribute to the finite part of scattering amplitudes at the corresponding loop order (so long as there are no factors of $1/\epsilon$ in their coefficients). Instead, they give rise to new linear relations between basis integrals up to corrections which vanish in a physical observable. These integrals have already found application within the method of differential equations [37,38], where they can be used to decouple systems near even integer dimensions.

Evanescently finite integrals feature a cancellation between an otherwise evanescent numerator (vanishing in four dimensions) and either UV or IR divergences, so that the singularities of the integrand are not locally integrable, but after integration one still obtains a finite result. Both evanescent and evanescently finite integrals are special to dimensional regularization, as both classes of integrals are ill defined in four dimensions. In contrast, locally finite integrals are well defined in four dimensions, and are expected to be independent of the UV and IR regulators.

In order to isolate finite integrals in a loop-momentum representation, we make use of Weinberg's theorem [39,40] to establish UV finiteness and on the time-honored approach of the Landau equations [41] to systematically identify all possible sources of IR divergences.[1] We use the techniques of Anastasiou and Sterman [29] to analyze the IR divergences of singular surfaces identified by the Landau equations. We introduce a compact set of variables that allows us to present the complete set of numerators yielding finite integrals in a simple form. As an example, we are able to describe the set of finite integrals to all loops for ladder topologies.

The rest of this paper is organized as follows. In Sec. II we review notation and ingredients for later sections. In Sec. III, we review Weinberg's theorem and conditions for UV finiteness. In Sec. IV we present well-known aspects of the theory of Landau singularities and then present our general algorithm to solve them and identify finite, evanescent, and evanescently finite integrals. In Sec. V we explain our approach using the one-loop box as an example. We continue in Sec. VI with a discussion of evanescent and evanescently finite integrands in more detail. We use the one-loop pentagon as an example. Our main results are collected in Sec. VII, where we show how to apply our techniques to increasingly complicated cases, up to four loops. In particular, we also demonstrate how choosing a basis of finite integrals helps make the singularities of the leading-color all-plus four-gluon amplitude manifest. We summarize in Sec. VIII. Explicit formulas can be found in the Appendixes.

II. NOTATION

We write an L-loop Feynman integral in dimensional regularization as

$$I[\mathcal{N}(\ell_i)] = \int \prod_{i=1}^{L} \mathrm{d}^D \ell_i \frac{\mathcal{N}(\ell_i)}{\mathcal{D}_1 \cdots \mathcal{D}_E}, \tag{1}$$

where $\mathcal{D}_e = q_e^2 - m_e^2 + i\varepsilon$ are the E propagators of the corresponding graph (with E edges) and $\mathcal{N}$ is a Lorentz-invariant numerator. The edge momenta q_e are linear combinations of the loop momenta ℓ_i and the external momenta k_j $(j = 1, \ldots, n)$ with coefficients ± 1 or 0. We consider integrals near four dimensions, $D = 4 - 2\epsilon$. The problem of classifying all finite integrals for a given graph

[1]The topic has recently enjoyed renewed interest, with exploration of new approaches to determining the locus of singular points associated to a given Feynman diagram [42–44].

(also called *topology*) can then be solved by finding all numerators $\mathcal{N}$ that make the integral (1) finite. Our goal is to identify the general form of $\mathcal{N}$.

Lorentz invariance requires numerators of Feynman integrals to be built out of scalar products of all available vectors: the loop momenta ℓ_i, the external momenta k_j, and any other external vectors Q_j independent of the loop momenta appearing in scattering amplitudes, such as polarization vectors. We take all external vectors to be strictly four dimensional. Numerators of Feynman integrals are then polynomials in $\ell_i \cdot \ell_j$, $\ell_i \cdot k_j$, and $\ell_i \cdot Q_j$ with coefficients that are rational functions of the external kinematic invariants. We can reduce scalar products of the form $\ell_i \cdot Q_j$ to combinations of $\ell_i \cdot \ell_j$ and $\ell_i \cdot k_j$ through a combination of standard tensor reduction and use of a basis for external vectors. This allows us to write any numerator in the form

$$\mathcal{N}(\ell_i) = \sum_{\vec{r}} c_{\vec{r}} \prod_a t_a^{r_a}, \tag{2}$$

where the t_a belong to the list of allowed scalar products described above,

$$t_a \in \{\ell_i \cdot k_j\} \cup \{\ell_i \cdot \ell_j\}, \tag{3}$$

and $\vec{r}$ are vectors of non-negative integer numbers representing the powers of each monomial. The coefficients c are rational functions of the kinematic invariants. In this article, we use the notation $k_{i\ldots j} \equiv k_i + \cdots + k_j$, and use as kinematic invariants the Mandelstam variables $s_{i\ldots j} = k_{i\ldots j}^2$ alongside the distinct nonzero masses: external $m_i^2 = k_i^2$ and internal m_e^2. Some masses may vanish, or be equal to other masses, as is the case for integrals arising in amplitudes.[2] In a slight abuse of language, we will refer to the total degree in the loop momenta as the rank of a term (rather than to the number of free indices); the rank of a numerator expression will be the maximum rank of any term.

The numerator representation given by Eqs. (2) and (3) is not unique. For our purposes, it will be useful to consider an alternative representation built using a van Neerven–Vermaseren basis, which we define below. We first define the generalized Gram determinant of two sets of R vectors in D dimensions,

$$G\begin{pmatrix} p_1 & \cdots & p_R \\ q_1 & \cdots & q_R \end{pmatrix} \equiv \det(2 p_i \cdot q_j),$$
$$G(\, p_1 \quad \cdots \quad p_R\,) \equiv G\begin{pmatrix} p_1 & \cdots & p_R \\ p_1 & \cdots & p_R \end{pmatrix}. \tag{4}$$

[2]In the literature on Feynman integrals, such configurations are sometimes called "exceptional/nongeneric kinematics."

We define a Gram with a free index,

$$G\begin{pmatrix} p_1 & \cdots \mu \cdots & p_R \\ q_1 & \cdots & q_R \end{pmatrix} \equiv \frac{\partial}{\partial w_\mu} G\begin{pmatrix} p_1 & \cdots w \cdots & p_R \\ q_1 & \cdots & q_R \end{pmatrix}. \tag{5}$$

Next, suppose that the space of external momenta for an n-point process is spanned by a basis $k_1, \ldots, k_R$, where $R = \min(n-1, 4)$ in four dimensions. The well-known van Neerven–Vermaseren basis can be defined as

$$v_i^\mu \equiv \frac{G\begin{pmatrix} k_1 & \cdots & \mu & \cdots & k_R \\ k_1 & \cdots & k_i & \cdots & k_R \end{pmatrix}}{G(\, k_1 \quad \cdots \quad p_R\,)}, \tag{6}$$

which has the important property,

$$v_i \cdot k_j = \delta_{ij} \quad \text{for } 1 \le j \le R, \tag{7}$$

and allows us to decompose any external momentum w^μ as

$$w^\mu = \sum_{j=1}^{R} (v_j \cdot w)\, k_j^\mu + \hat{w}^\mu, \tag{8}$$

with $k_i \cdot \hat{w} = 0$ for $i = 1, \ldots, R$. The remainder $\hat{w}$ satisfies $\hat{w}^2 \le 0$. In the rest of this manuscript we will reserve the "hat" symbol for out-of-plane components of momenta.

We also introduce $\widehat{\ell}_i$, the out-of-plane part of the loop momentum ℓ_i orthogonal to all external momenta k_j. When considering an n-point process with $n > 4$, this part is strictly ϵ dimensional. Using Eq. (8) we can then write the scalar products in Eq. (3) as linear combinations of those in the set,

$$t_a \in \{\ell_i \cdot v_j\} \cup \{\widehat{\ell}_i \cdot \widehat{\ell}_j\}, \tag{9}$$

which span the same space as the one generated by Eq. (3) but greatly simplify the identification of IR-finite numerators. This alternate basis will allow us to generalize our analysis more easily than the standard basis in Eq. (3). It is convenient to define the notation,

$$\nu_{ij} \equiv \widehat{\ell}_i \cdot \widehat{\ell}_j = G\begin{pmatrix} l_i & k_1 & \cdots & k_R \\ l_j & k_1 & \cdots & k_R \end{pmatrix} \Big/ G\begin{pmatrix} k_1 & \cdots & k_R \\ k_1 & \cdots & k_R \end{pmatrix}. \tag{10}$$

Conveniently, all definitions above can be continued to D continuous space-time dimensions, whenever necessary.

With the notation and numerator representations in hand, we turn to the constraints on Eq. (2) imposed by UV and IR finiteness. We consider UV constraints in the next section, and IR constraints in following sections.

III. UV DIVERGENCES AND WEINBERG'S THEOREM

The UV divergences of a Feynman integral arise from regions where loop momenta become large. The convergence criterion known today as Weinberg's theorem was introduced by Dyson [39] and proven rigorously by Weinberg [40] in the case of a Euclidean metric. A simpler proof and an extension to the Minkowski case was presented by Hahn and Zimmermann [45], while Nakanishi gave a proof based on the parametric representation [46].

The power-counting theorem states that a Feynman integral is UV finite if the integral itself as well as all its subintegrations have a negative superficial degree of divergence. Subintegration here means integrating over at most $(L-1)$ independent loops of the graph while keeping the remaining propagator momenta fixed to generic values.

For any given subintegration, we can always redefine the loop-momentum variables so that they correspond to integration over a proper subset S of the loop momenta ℓ_i holding the remaining ones fixed. Rescaling the unfixed loop momenta in S as $\ell^\mu \to \rho\,\ell^\mu$ with $\rho \gg 1$, we find that the product of integrand and measure scales as ρ^ω, where ω is the superficial degree of divergence of the subintegration.

Below we show explicitly how Weinberg's theorem can be used in practice to constrain a generic integral like the one in Eq. (1). We take the simple two-loop "kite" integral shown in Fig. 1 as an example.

Requiring the superficial convergence ($\omega < 0$) of the whole integral puts an upper bound on the numerator rank:

$$\mathrm{rank}(\mathcal{N}) \le r_{\max} = 2E - 4L - 1. \tag{11}$$

For Fig. 1, the rescaling $\ell_{1,2} \to \rho\ell_{1,2}$ gives a superficial degree of divergence $\omega = \mathrm{rank}(\mathcal{N}) - 2$, which implies $\mathrm{rank}(\mathcal{N}) \le 1$: the numerator can be at most linear in the loop momenta.

Requiring convergence of subintegrations puts additional constraints on the numerator. To find them, we first need to identify all possible subintegrations. For simple examples like the one considered here, it is convenient to work in momentum space and what follows is one way of doing this algorithmically.[3]

We start by listing all distinct linear combinations $c_i^{(v)}\ell_i$ of loop momenta entering the denominators (equivalently, the set of all propagator momenta evaluated at vanishing internal masses and external momenta). We then pick a subset V of these linear combinations $\{c_i^{(v)}\ell_i \in V\}$, and fix each element in the subset to a different constant,

[3]As we shall discuss in Sec. IV B, we analyze more complicated integrals in Feynman parameter space. One can then solve the equations obtained by setting the first Symanzyk polynomial to zero monomial by monomial in order to identify the "unfixed" edges.

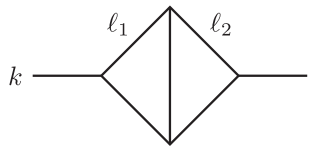

FIG. 1. A simple two-loop two-point integral.

$$c_i^{(v)}\ell_i = d_v, \quad \forall\ v \in V, \tag{12}$$

and solve the corresponding system of equations for the loop momenta. We retain only subsets which leave at least one ℓ_i unconstrained. In the kite integral, the different linear combinations of loop momenta are $\{\ell_1, \ell_2, \ell_1+\ell_2\}$, while the list of subsets and their corresponding constraints is

$$\begin{aligned}&\{\ell_1 = d_1, \ell_2 = d_2\},\ \{\ell_1 = d_1, \ell_1+\ell_2 = d_2\},\\ &\qquad \{\ell_2 = d_1, \ell_1+\ell_2 = d_2\},\\ &\{\ell_1 = d\},\ \{\ell_2 = d\},\ \{\ell_1+\ell_2 = d\}.\end{aligned} \tag{13}$$

The subsets in the top row leave no loop momentum unconstrained. Conversely, each of the subsets in the bottom row leaves 1 degree of freedom unfixed and therefore corresponds to a subintegration. Graphically, these three subsets can be associated to the diagrams shown in Fig. 2.

With the set of subintegrations at hand, we turn to finding the corresponding additional constraints on the numerator. We write down the most general *Ansatz* with the maximal allowed overall rank $r_{\max}$ as a linear combination of all possible monomials. This is equivalent to setting to zero all coefficients $c_{\vec{r}}$ with $\sum_a r_a > r_{\max}$ in the general *Ansatz* of Eq. (2). It turns the infinite-dimensional space of polynomials into a finite-dimensional space of superficially UV-convergent numerators:

$$\sum_{\vec{r}} c_{\vec{r}} \prod_a t_a^{r_a} \quad \text{where} \sum_a r_a \le r_{\max}. \tag{14}$$

For each subintegration we substitute the corresponding solution in Eq. (12) into the general numerator, and rescale all unfixed loop momenta as $\ell \to \rho\,\ell$. We then expand the numerator in the scaling parameter ρ, and require that the divergent orders in ρ vanish. This yields a system of linear equations. Solving them for $c_{\vec{r}}$ gives the most general numerator consistent with UV finiteness. In the kite example, the set of monomials is $\{\ell_1\cdot\ell_2, \ell_1\cdot k, \ell_2\cdot k\}$, which give the superficially UV-convergent numerator,

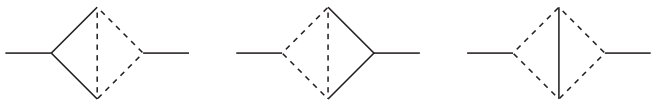

FIG. 2. Graphical depiction of subintegrations for the integral in Fig. 1. The active subintegrations are indicated by dashed lines, while the momenta corresponding to solid lines are kept fixed.

$$\mathcal{N} = c_{(0,1,0)}\ell_1 \cdot k + c_{(0,0,1)}\ell_2 \cdot k. \tag{15}$$

The three subintegrations of Fig. 2 provide respectively the scaling rules,

$$\{\ell_1 = d, \ell_2 \to \rho\ell_2\},\ \{\ell_1 \to \rho\ell_1, \ell_2 = d\},\ \{\ell_1 = d - \ell_2, \ell_2 \to \rho\ell_2\}, \tag{16}$$

which impose no further constraint on the numerator in Eq. (15).

Weinberg's criterion gives a sufficient condition for UV finiteness, but not a necessary one. Integrals which have a UV divergence by power counting may have the coefficient of that singularity vanish because of cancellations. We denote an application of Weinberg's criterion as *strong* UV convergence, and a vanishing coefficient of a potential UV divergence as *weak* UV convergence. In this article we consider only integrands giving strongly UV convergent integrals. In a purely numerical evaluation, the former can be evaluated stably, while the latter would still require a regulator.

IV. IR DIVERGENCES, LANDAU EQUATIONS, AND POWER COUNTING

A. Potential singularities: The Landau equations

Infrared divergences of Feynman integrals are associated to loop-momentum configurations in which a subset of the propagators (equivalently a subset of the denominators) in Eq. (1) vanish. In general, the domain of integration of an L-loop Feynman integral (1) with E propagators will contain IR-divergent surfaces of various dimensions. These correspond to solutions of the Landau equations [41] (see also Ref. [47] for an up-to-date literature review and Refs. [21,48] for a pedagogical discussion of IR divergences). In presenting the Landau equations, it is convenient to rewrite the integral of Eq. (1) in the mixed representation[4]:

$$I[\mathcal{N}(\ell_i)] = \Gamma(E) \int \prod_{i=1}^{L} \mathrm{d}^D\ell_i \int_0^\infty \frac{\prod_{e=1}^{E} \mathrm{d}\alpha_e}{\mathrm{GL}(1)} \times \frac{\mathcal{N}(\ell_i)}{[\alpha_1\mathcal{D}_1 + \cdots + \alpha_E\mathcal{D}_E]^E}, \tag{17}$$

where the GL(1) denominator accounts for the projective invariance of the integration over the Feynman parameters α_e. It is equivalent to the usual notation $\delta(1 - \sum_{e\in A}\alpha_e)$ with A a subset of $\{1, \ldots, E\}$. Potential singularities of the integral correspond to configurations of the integration variables[5] which satisfy,

$$\forall\ i = 1, \ldots, L: \quad \sum_{e=1}^{E} \alpha_e \frac{\partial}{\partial\ell_i}\mathcal{D}_e = 0, \tag{18a}$$

$$\forall\ e = 1, \ldots, E: \quad \alpha_e\mathcal{D}_e = 0. \tag{18b}$$

These are the Landau equations, which should be viewed as a system of equations for the loop momenta and the kinematic invariants for some values of $\alpha_e \geq 0$ where at least one α_e is strictly positive.

There are two classes of solutions to the Landau equations. Solutions of the first class impose constraints on the kinematic variables. Such solutions manifest themselves as singularities of the integrals as a function of these variables, and are called *Landau singularities*. Kinematics-independent solutions, on the other hand, correspond to IR divergences, and manifest themselves as poles in the dimensional regulator ϵ. In what follows we will only be concerned with the latter class of solutions.

B. Solving the Landau equations

The set of equations (18a) are linear in the loop momenta, while (18b) are quadratic. We proceed by first solving the linear system (18a) for the loop momenta, expressing them in terms of the external momenta and the α parameters. We then substitute the solution into the remaining Eq. (18b), and obtain a system of polynomial equations for the α parameters. In many cases the latter system can be solved easily, as we will see below.

This procedure relates the Landau equations to the Symanzik polynomials of the Feynman graph (see Refs. [46,50]),

$$\mathcal{U}(\alpha) = \sum_{T\in\mathcal{T}_1} \prod_{e\notin T} \alpha_e, \tag{19a}$$

$$\mathcal{F}(\alpha) = \sum_{T\in\mathcal{T}_2} k(T)^2 \prod_{e\notin T}\alpha_e - \mathcal{U}(\alpha)\sum_{e=1}^{E} m_e^2\alpha_e, \tag{19b}$$

where $\mathcal{T}_n$ is the set of spanning n forests of the graph, and $k^\mu(T)$ is the total momentum flowing across the two-forest $T \in \mathcal{T}_2$. The Symanzik polynomials can be computed efficiently by rewriting the combined denominator in the mixed representation as a quadratic form in the loop momenta:

$$\sum_{e=1}^{E} \alpha_e\mathcal{D}_e = \sum_{i,j=1}^{L} A_{ij}\ell_i \cdot \ell_j - 2\sum_{i=1}^{L} \ell_i \cdot B_i + C, \tag{20}$$

so that

$$\mathcal{U} = \det A, \tag{21a}$$

$$\mathcal{F} = \det A(-B^T A^{-1} B + C). \tag{21b}$$

[4]In the classic book [49], it is called the "second representation".

[5]We except UV singularities, which we assume have already been removed.

An immediate consequence of Eqs. (20) and (21a) is that the linear system (18a) is nondegenerate if and only if $\mathcal{U} \neq 0$. Let us consider this nondegenerate case first. As the square matrix A is of full rank, the linear system (18a) admits a unique solution,

$$\ell_i^\mu = (A^{-1})_{ij} B_j^\mu. \tag{22}$$

(A parametrization-independent form of the solution in terms of the graph spanning trees can be found in Ref. [47].) We now substitute this solution into the quadratic equations (18b), which become simply

$$\forall\ = 1, \ldots, E: \qquad \alpha_e \frac{\partial}{\partial \alpha_e} \mathcal{F} = 0. \tag{23}$$

These equations are *also* sometimes referred to as "the Landau equations"; they describe singularities of the integrand in the Feynman-parameter representation[6] when $\mathcal{U} \neq 0$.[7]

To solve Eq. (23), observe that, due to Euler's homogeneous function theorem, Eq. (23) implies $\mathcal{F} = 0$. In many cases, $\mathcal{F}$ can be brought into a *subtraction-free* form, meaning that each monomial in $\mathcal{F}$ has the same sign in a certain region of the kinematic space (equivalently, there exists a Euclidean region[8] of the integral). In particular, this holds for planar Feynman graphs with massless external legs. In these cases the $k(T)^2$ in Eq. (19b) are Mandelstam invariants of consecutive external momenta (with respect to the planar ordering), which can be made negative simultaneously (in general using complex momenta).

For $\alpha_e \geq 0$, a subtraction-free polynomial $\mathcal{F}$ can only vanish if each monomial in $\mathcal{F}$ vanishes independently, which in turn implies Eq. (23). Therefore, for a subtraction-free $\mathcal{F}$, solving Eq. (23) is equivalent to setting all monomials in $\mathcal{F}$ to zero independently. The solutions have the form

$$\alpha_{e_1} = 0, \ldots, \alpha_{e_m} = 0, \tag{24}$$

where $e_1, \ldots, e_m$ is a proper subset of edge labels $\{1, \ldots, E\}$.

When $\mathcal{F}$ does not admit a subtraction-free form, we must solve Eq. (23) explicitly. It is believed that the general form of the solution in such cases is nonetheless also given by Eq. (24). That is, IR divergences cannot arise due to cancellation between terms in $\mathcal{F}$.

One possible strategy to prove this for a given diagram is as follows. Instead of summing Eq. (23) to get $\mathcal{F} = 0$, which is not subtraction free, consider the most general linear combination of Eq. (23):

$$\sum_{e=1}^{E} w_e \alpha_e \frac{\partial}{\partial \alpha_e} \mathcal{F} = 0. \tag{25}$$

The left-hand side of Eq. (25) contains the same monomials as $\mathcal{F}$, but the coefficients of these monomials are now linear functions of w_e. Demanding that all coefficients are nonzero and have the same sign in some region of the kinematic space, one obtains a system of linear inequalities on w_e. If one can find a solution of this system (e.g., using numerical linear optimization routines), then solving Eq. (23) is equivalent to setting each monomial in $\mathcal{F}$ to zero independently as in the subtraction-free case, therefore no cancellations can occur. We illustrate this procedure in Sec. VII C when we discuss the massless nonplanar double-box integral.

Having solved the parameter-space Landau equations (23), it remains to check that the solution is consistent with the condition $\mathcal{U} \neq 0$, and compute the corresponding loop momenta using Eq. (22).

We turn next to the degenerate case, $\mathcal{U} = 0$. As we can see from Eq. (19a), $\mathcal{U}$ is always subtraction free, so this condition implies that a subset of α_e vanishes, and all such subsets are identified by setting all monomials in $\mathcal{U}$ to zero. Each solution of $\mathcal{U} = 0$ corresponds to the situation where a subdiagram γ of the original graph G (formed by the edges for which $\alpha_e = 0$) does not contribute to the Landau equations; effectively, they turn into analogous equations for the *reduced diagram* G/γ obtained by contracting the subdiagram γ to a point. This means that solutions of the Landau equations in the degenerate case can be found by recursively solving the nondegenerate equations for the reduced diagrams.

A convenient way to implement this in a computer code is by using the following factorization formulas for the Symanzik polynomials (for example, see Proposition 4.1 of Ref. [42] and references therein):

$$\mathcal{U}_G|_{\alpha_\gamma \to \lambda \alpha_\gamma} = \lambda^{L_\gamma} \mathcal{U}_\gamma \mathcal{U}_{G/\gamma} + \mathcal{O}(\lambda^{L_\gamma + 1}), \tag{26a}$$

$$\mathcal{F}_G|_{\alpha_\gamma \to \lambda \alpha_\gamma} = \lambda^{L_\gamma} \mathcal{U}_\gamma \mathcal{F}_{G/\gamma} + \mathcal{O}(\lambda^{L_\gamma + 1}), \tag{26b}$$

where $\alpha_\gamma \to \lambda \alpha_\gamma$ means that α_e are replaced by $\lambda \alpha_e$ for all edges in γ, while L_γ is the number of loops in the subdiagram γ. Equation (26a) also shows that $\mathcal{U}$ vanishes only when γ contains at least one loop, so the degenerate case $\mathcal{U} = 0$ actually corresponds to IR subdivergences with one or more loop momenta unconstrained.

The procedure just described for solving the Landau equations can be summarized as follows:

[6]This is the "third representation" of Ref. [49].

[7]A version of Eq. (23) which captures also the singularities with $\mathcal{U} = 0$ is obtained by replacing $\mathcal{F}$ with the *worldline action* $\mathcal{F}/\mathcal{U}$ suitably continued to the boundary (Remark 9.2 and Theorem 12.1 of [46].

[8]The same term is sometimes used to refer to a region where *all* Mandelstam variables are positive. This is not possible in general for scattering processes when all external states are massless.

(1) Compute the first Symanzik polynomial $\mathcal{U}$ using Eq. (21a).
(2) Recursively find all reduced diagrams with one or more loops contracted to a point by solving the equation $\mathcal{U}=0$ monomial by monomial, and using Eq. (26a) to evaluate $\mathcal{U}$ for reduced diagrams.
(3) For the original diagram and each reduced diagram:
   (a) compute the second Symanzik polynomial $\mathcal{F}$ using Eqs. (21b) and (26b);
   (b) if $\mathcal{F}$ is subtraction free, solve $\mathcal{F}=0$ monomial by monomial, otherwise solve Eq. (23) explicitly, e.g., by finding a subtraction-free linear combination (25); and
   (c) keep only solutions for which the corresponding $\mathcal{U}\neq 0$.
(4) For each solution, which is given as a set of equality constraints on α_e, evaluate the corresponding constraints on the loop momenta using Eq. (22). These constraints describe the sought-after surfaces in the loop momentum space which contain all IR divergences.

C. IR power counting

Solutions of the Landau equations turn out to impose two types of constraints on the loop momenta: *soft* constraints take the form $q_e(\ell,k)=0$, where $q_e(\ell,k)$ is the momentum of a massless line, while *collinear* constraints require $q_e(\ell,k)=xk_i$, where k_i is an external massless momentum, and the proportionality coefficient $x\in(0,1)$ is the ratio of unconstrained α parameters, such as $\alpha_1/(\alpha_1+\alpha_2)$.

Following Anastasiou and Sterman [29], we use the IR power-counting technique of Libby and Sterman [51] to determine the behavior of the integral near a divergent surface described by soft and collinear constraints. Namely, we parametrize the vicinity of the divergent surface by modifying the constraints as follows:

$$\begin{aligned} q_e^\mu(\ell,k)=0 \quad &\to \quad q_e^\mu(\ell,k)=\lambda\sigma_e^\mu,\\ q_e^\mu(\ell,k)=x_e k_i^\mu \quad &\to \quad q_e^\mu(\ell,k)=x_e k_i^\mu+\lambda\eta_i^\mu+\lambda^{1/2}q_e^{\perp,\mu}. \end{aligned} \tag{27}$$

Here, $\bar{q}_e$ is a unit Euclidean-norm vector while η_i and $q_e^\perp$ satisfy

$$q_e^\perp\cdot k_i=\eta_i^2=q_e^\perp\cdot\eta_i=0 \quad \text{and} \quad \hat{\eta}_i=0. \tag{28}$$

Solving the modified set of constraints for the loop momenta, we obtain a scaling rule of the form $\ell_i=\ell_i(\lambda)$, which can be used to find numerators canceling the divergence the same way as we did in the UV case. For every divergent configuration of the loop momenta, we can substitute the scaling rules of Eq. (27) into the integration measure, which yields

$$\begin{aligned} \text{soft}:\ \mathrm{d}^D\ell &= \mathrm{d}\Omega_D\,\mathrm{d}\lambda\,\lambda^{D-1}\sim\mathrm{d}\lambda\,\lambda^{D-1},\\ \text{collinear}:\ \mathrm{d}^D\ell &= \frac{1}{2}\mathrm{d}x_e\,\mathrm{d}^2q_e^\perp\mathrm{d}\Omega_{D-2}(k_i\cdot\eta_i)\mathrm{d}\lambda\,\lambda^{D/2-1}\\ &\sim\mathrm{d}\lambda\,\lambda^{D/2-1}, \end{aligned} \tag{29}$$

as well as into the integrand obtained from the UV-compatible numerator obtained in the previous section. We then Laurent expand the integrand in λ and retain only powers leading to divergences. The coefficients of divergent powers of λ are in general polynomials in the quantities

$$\begin{aligned} &\ell_i\cdot v_j,\quad \nu_{ij},\quad \hat{\ell}_i\cdot\hat{\sigma}_e,\quad \hat{\ell}_i\cdot\hat{q}_j^\perp,\quad v_i\cdot q_j^\perp,\quad v_i\cdot\eta_j,\\ &v_i\cdot\sigma_e,\quad \hat{\sigma}_e\cdot\hat{q}_j^\perp,\quad \hat{q}_i^\perp\cdot\hat{q}_j^\perp,\quad \hat{\sigma}_{e_1}\cdot\hat{\sigma}_{e_2},\quad x_e, \end{aligned} \tag{30}$$

with coefficients depending on the *Ansatz* parameters $c_{\vec{r}}$, and ℓ_i being the unconstrained loop momenta. The set of monomials in Eq. (30) is determined by substituting the modified constraints of Eq. (27) into the *Ansätze* of Eqs. (2) and (9).

However, not all monomials in Eq. (30) are independent. We can find relations by applying the decomposition of Eq. (8) to each of the vectors appearing in Eq. (28). We find

$$\begin{aligned} \sum_{j=1}^{R}(k_i\cdot k_j)\,v_j\cdot q_e^\perp &= \sum_{j,h=1}^{R}(k_j\cdot k_h)\,v_j\cdot\eta_i\,v_h\cdot\eta_i\\ &= \sum_{j,h=1}^{R}(k_j\cdot k_h)\,v_j\cdot q_e^\perp\,v_h\cdot\eta_i=0, \end{aligned} \tag{31}$$

with i labeling a massless external momentum k_i. The first is a relation among degree-1 monomials while the other two are among degree-2 monomials. We take these relations into account and require that the coefficient of every independent monomial should vanish. The solution of the associated system of equations leads us to a set of constraints on the *Ansatz* parameters.

The $k_i\cdot k_j$ factors appearing in Eq. (31) are the only kinematics-dependent objects which enter the system of linear equations induced by the IR finiteness constraints. Moreover, they are only relevant when powerlike collinear singularities are present. In practice, one can first solve the system of equations which does not involve these $k_i\cdot k_j$ and then solve a much smaller system coming from the subleading contributions of the numerator which may possibly depend on the $k_i\cdot k_j$. This greatly simplifies the determination of locally finite numerators and allows us to compute them for topologies up to four loops on a laptop. In practice when the problem involves large systems of equations we use FiniteFlow [52] to obtain a solution efficiently.

Repeating the procedure above for all IR-divergent surfaces, we find the most general numerator consistent

with IR finiteness for a given *Ansatz*. Denoting the space of locally finite numerators by $\mathcal{W}$, any element $f \in \mathcal{W}$ can then be written in the form

$$f(\ell) = \sum_i g_i \mathcal{N}_i(\ell), \tag{32}$$

where the $\mathcal{N}_i$ are polynomials in the independent monomials in Eq. (9) and the g_i are unconstrained coefficients independent of the loop momenta.

To guarantee IR finiteness, following Ref. [29], one must check not only the divergent surfaces found from the Landau analysis, but also subsurfaces. The latter do not always show up as separate solutions of the Landau equations. In particular, a solution with a soft constraint may be a special case of a solution with a collinear constraint when the proportionality coefficient x_e reaches its boundary value of 0 or 1. To include the subsurfaces we also consider each solution of the Landau equations where x_e have been set to 0 or 1 in all possible combinations. This is necessary only when the degree of divergence of a subsurface is greater than that of any of the parent surfaces. An example of this would be a set of surfaces associated to logarithmic divergences intersecting on a subsurface which leads to a powerlike divergence, as in the case of the massless nonplanar double box, see Sec. VII C.

D. Finite integral generators

Suppose we have the set of all locally IR-finite numerators $\widetilde{\mathcal{W}}$, constructed as above without imposing UV finiteness. Multiplying any locally IR-finite numerator $f \in \widetilde{\mathcal{W}}$ by any polynomial p in the variables of Eq. (9) yields another locally IR-finite numerator:

$$pf \in \widetilde{\mathcal{W}}. \tag{33}$$

This is the defining property of an *ideal*; it implies that there exists a (nonunique) minimal set of polynomials $f_1, f_2, \ldots \in \mathcal{W}$ which generate $\widetilde{\mathcal{W}}$:

$$\widetilde{\mathcal{W}} = \langle f_1, f_2, \ldots \rangle. \tag{34}$$

This means that any IR-finite polynomial can be written as a linear combination of $f_1, f_2, \ldots$ with polynomial coefficients, and vice versa, any such combination is IR finite. As we shall see, only a small number of generators are required. This allows us to capture all information on $\widetilde{\mathcal{W}}$ in a very compact form.

Requiring UV finiteness then restricts us to a finite-dimensional subspace within the ideal. We will call this the *truncated ideal* of locally finite numerators, though it is mathematically no longer an ideal. We will order generators according to their UV behavior, favoring numerators with lower degrees in the loop momenta.

One could of course impose the UV-finiteness and IR-finiteness conditions in either order; we will impose the UV-finiteness ones first. The set of generators we obtain will be the same.

V. A SIMPLE EXAMPLE: ONE-LOOP BOX

To illustrate the procedure described in the previous sections, let us consider the one-loop massless box integral, depicted in Fig. 3, as a simple example. We define the momenta,

$$q_1 = \ell, \quad q_2 = \ell - k_1, \quad q_3 = \ell - k_{12}, \quad q_4 = \ell - k_{123}. \tag{35}$$

We start by writing down the most general *Ansatz* for a UV-finite numerator as described in Sec. III. Superficial convergence imposes a maximum degree $r_{\max} = 3$ and as there are no subintegrations the *Ansatz* reads

$$\begin{aligned}\mathcal{N}(\ell) = {} & c_0 + c_1\, \ell\cdot v_1 + c_2\, \ell\cdot v_2 + c_3\, \ell\cdot v_3 + c_4\, \hat{\ell}^2 + c_5\, (\ell\cdot v_1)^2 + c_6\, \ell\cdot v_1\, \ell\cdot v_2 \\ & + c_7\, (\ell\cdot v_2)^2 + c_8\, \ell\cdot v_1\, \ell\cdot v_3 + c_9\, \ell\cdot v_2\, \ell\cdot v_3 + c_{10}\, (\ell\cdot v_3)^2 + c_{11}\, \hat{\ell}^2\, \ell\cdot v_1 \\ & + c_{12}\, \hat{\ell}^2\, \ell\cdot v_2 + c_{13}\, \hat{\ell}^2\, \ell\cdot v_3 + c_{14}\, (\ell\cdot v_1)^3 + c_{15}\, (\ell\cdot v_1)^2\, \ell\cdot v_2 \\ & + c_{16}\, \ell\cdot v_1\, (\ell\cdot v_2)^2 + c_{17}\, (\ell\cdot v_2)^3 + c_{18}\, (\ell\cdot v_1)^2\, \ell\cdot v_3 + c_{19}\, \ell\cdot v_1\, \ell\cdot v_2\, \ell\cdot v_3 \\ & + c_{20}\, (\ell\cdot v_2)^2\, \ell\cdot v_3 + c_{21}\, \ell\cdot v_1\, (\ell\cdot v_3)^2 + c_{22}\, \ell\cdot v_2\, (\ell\cdot v_3)^2 + c_{23}\, (\ell\cdot v_3)^3. \end{aligned} \tag{36}$$

Moving to the IR analysis, we start by computing the auxiliary quantities [see Eq. (20)],

$$\begin{aligned} A_{11} &= \alpha_1 + \alpha_2 + \alpha_3 + \alpha_4, \\ B_1^\mu &= (\alpha_2 + \alpha_3 + \alpha_4)\, k_1^\mu + (\alpha_3 + \alpha_4)\, k_2^\mu + \alpha_4\, k_3^\mu, \end{aligned} \tag{37}$$

so that the Symanzik polynomials for this diagram are

$$\mathcal{U} = \alpha_1 + \alpha_2 + \alpha_3 + \alpha_4, \qquad \mathcal{F} = s\,\alpha_1\alpha_3 + t\,\alpha_2\alpha_4. \tag{38}$$

Solving $\mathcal{F} = 0$ monomial by monomial, and then using Eq. (22) together with Eq. (37), we obtain four solutions corresponding to divergent surfaces of collinear type. Intersecting these surfaces, or equivalently setting the proportionality coefficients to 0 or 1, we find four soft subsurfaces. We list the results in Table I.

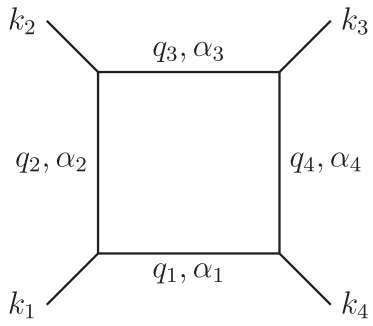

FIG. 3. The massless one-loop box graph.

To each of the singular configurations we associate a modified constraint $\ell = \ell(\lambda)$ as described in Eq. (27) and substitute it into the momentum-space representation of the integral,

$$\mathrm{Box}[\mathcal{N}(\ell)] = \int \mathrm{d}^D\ell \frac{\mathcal{N}(\ell)}{\mathcal{D}_1\mathcal{D}_2\mathcal{D}_3\mathcal{D}_4}. \tag{39}$$

Using the integration-measure scalings (29) together with the scaling of the propagators $\mathcal{D}_e = q_e^2 + i\varepsilon$, we find that Box [1] behaves as $\mathrm{d}\lambda\,\lambda^{-1+\mathcal{O}(\epsilon)}$ near $D = 4$ for all the soft and collinear configurations of Table I. Because of the logarithmic nature of these singularities, we need to expand the numerator only to $\mathcal{O}(\lambda^0)$ to obtain singular contributions to the integral. To this order in λ we find that the monomials $\{\hat{\ell}^2, \ell\cdot v_1, \ell\cdot v_2, \ell\cdot v_3\}$ take the values

$$\begin{aligned} &C_1\colon \{0, x_1, 0, 0\}, \quad C_2\colon \{0, 1, x_2, 0\}, \quad C_3\colon \{0, 1, 1, x_3\}, \quad C_4\colon \{0, x_4, x_4, x_4\}, \\ &S_1\colon \{0, 0, 0, 0\}, \quad S_2\colon \{0, 1, 0, 0\}, \quad S_3\colon \{0, 1, 1, 0\}, \quad S_4\colon \{0, 1, 1, 1\}, \end{aligned} \tag{40}$$

where the x_e stand for the collinear-fraction parameters which can be read off from Table I for the different collinear regions.

Let us study these configurations, extracting the corresponding constraints on the numerator. Substituting the collinear configurations into Eq. (36) and setting the result to zero for every value of the x_e we find the equations,

TABLE I. Solutions of the Landau equations for the one-loop box and the corresponding IR divergent surfaces and subsurfaces. Dotted lines indicate collinear subdiagrams while dashed lines represent soft propagators.

Surface	Solution of $\mathcal{F} = 0$	Momentum constraint	Subsurface	Momentum constraint
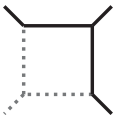 (C_1)	$\alpha_3 = \alpha_4 = 0$	$q_1 = \frac{\alpha_2}{\alpha_1+\alpha_2} k_1$	 $(S_1) = (C_4) \cap (C_1)$	$q_1 = 0$
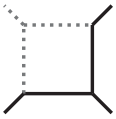 (C_2)	$\alpha_4 = \alpha_1 = 0$	$q_2 = \frac{\alpha_3}{\alpha_2+\alpha_3} k_2$	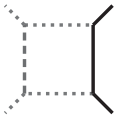 $(S_2) = (C_1) \cap (C_2)$	$q_2 = 0$
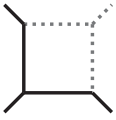 (C_3)	$\alpha_1 = \alpha_2 = 0$	$q_3 = \frac{\alpha_4}{\alpha_3+\alpha_4} k_3$	 $(S_3) = (C_2) \cap (C_3)$	$q_3 = 0$
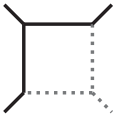 (C_4)	$\alpha_2 = \alpha_3 = 0$	$q_4 = \frac{\alpha_1}{\alpha_4+\alpha_1} k_4$	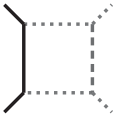 $(S_4) = (C_3) \cap (C_4)$	$q_4 = 0$

$$
\begin{aligned}
&C_1\colon\ c_0 = c_1 = c_5 = c_{14} = 0,\\
&C_2\colon\ c_0 + c_1 + c_5 + c_{14} = c_2 + c_6 + c_{15} = c_7 + c_{16} = c_{17} = 0,\\
&C_3\colon\ c_0 + c_1 + c_2 + c_5 + c_6 + c_7 + c_{14} + \cdots + c_{17}\\
&\quad = c_3 + c_8 + c_9 + c_{18} + c_{19} + c_{20} = c_{10} + c_{21} + c_{22} = c_{23} = 0,\\
&C_4\colon\ c_0 = c_1 + c_2 + c_3 = c_5 + \cdots + c_{10} = c_{14} + \cdots + c_{23} = 0.
\end{aligned} \tag{41}
$$

As anticipated these equations do not depend on the external kinematic invariants s_{ij}. Moving on, for each soft region S_i we get the following constraints:

$$
\begin{aligned}
&S_1\colon\ c_0 = 0,\\
&S_2\colon\ c_0 + c_1 + c_5 + c_{14} = 0,\\
&S_3\colon\ c_0 + c_1 + c_2 + c_5 + c_6 + c_7 + c_{14} + \cdots + c_{17} = 0,\\
&S_4\colon\ c_0 + \cdots + c_3 + c_5 + \cdots + c_{10} + c_{14} + \cdots + c_{23} = 0.
\end{aligned} \tag{42}
$$

One can check that these constraints are satisfied automatically if Eq. (41) holds. This comes as no surprise, because in this case soft subsurfaces have the same degree of divergence as their parent surfaces corresponding to collinear regions (see the discussion at the end of Sec. IV C). Therefore, cancellation of collinear divergences is sufficient for IR finiteness.

The constraints in Eqs. (41) and (42) entirely fix 12 coefficients in the *Ansatz* of Eq. (36). Therefore, within the space of UV-finite numerators of Eq. (36), described by 24 independent monomials, the subset of IR-finite integrals has 12 degrees of freedom.

In general, the results of a UV-IR analysis such as the one presented above can be summarized by simply listing the generators of the ideal of IR-finite numerators. A set of generators can be found using standard techniques of computational algebraic geometry, such as Gröbner bases, and then prettifying the results. In the case of the massless one-loop box there are only three rank-two generators: $\hat{\ell}^2$, $(\ell - k_1)\cdot v_1\, \ell\cdot(v_2 - v_3)$ and $\ell\cdot v_3\, \ell\cdot(v_1 - v_2)$. Using them we can write the most general UV- and IR-finite numerator for the massless one-loop box as

$$
\begin{aligned}
\mathcal{N}(\ell) = {}& [b_1 + b_2 \ell\cdot v_1 + b_3 \ell\cdot v_2 + b_4 \ell\cdot v_3](\ell - k_1)\cdot v_1\, \ell\cdot(v_2 - v_3)\\
&+ [b_5 + b_6 \ell\cdot v_1 + b_7 \ell\cdot v_2 + b_8 \ell\cdot v_3]\ell\cdot v_3\, \ell\cdot(v_1 - v_2)\\
&+ [b_9 + b_{10} \ell\cdot v_1 + b_{11} \ell\cdot v_2 + b_{12} \ell\cdot v_3]\hat{\ell}^2,
\end{aligned} \tag{43}
$$

where the b_i are purely functions of the external momenta.

We end our discussion with two comments on Eq. (43):

(1) The generators obtained in the van Neerven–Vermaseren basis of monomials have a straightforward representation in terms of Gram determinants,

$$
\begin{aligned}
(\ell - k_1)\cdot v_1\, \ell\cdot(v_2 - v_3) &\propto G\begin{pmatrix} \ell - k_1 & 2 & 3 \\ 1 & 2 & 3 \end{pmatrix} G\begin{pmatrix} \ell & 1 & 4 \\ 1 & 2 & 3 \end{pmatrix},\\
\ell\cdot v_3\, \ell\cdot(v_1 - v_2) &\propto G\begin{pmatrix} \ell & 1 & 2 \\ 1 & 2 & 3 \end{pmatrix} G\begin{pmatrix} \ell & 3 & 4 \\ 1 & 2 & 3 \end{pmatrix},\\
\hat{\ell}^2 &\propto G\begin{pmatrix} \ell & 1 & 2 & 3 \end{pmatrix},
\end{aligned} \tag{44}
$$

where the constants of proportionality depend only on the external momenta (here and in what follows we represent the external momenta k_i inside the Gram determinants with the corresponding labels i). This observation generalizes to higher loops.

(2) Equation (43) is just one possible choice to represent the same numerator. For instance, one could swap the $\ell \cdot v_i$ factors inside the brackets in Eq. (43) for $\ell \cdot k_i$ or rewrite them in terms of inverse propagators where possible. As long as the UV power counting is satisfied, one can choose different representations depending on the context.

VI. EVANESCENT INTEGRANDS

Locally finite integrals, enumerated by the algorithmic procedure described above, contain a noteworthy subset of integrals which are manifestly of $\mathcal{O}(\epsilon)$ while containing no explicit appearances of ϵ (or D). We call these *evanescent* integrals. To find integrands giving rise to evanescent integrals, we start with the set of integrands of locally finite integrals, and impose further restrictions on their coefficients. In particular, we can split the numerator of the integrand,

$$\mathcal{N} = \mathcal{N}_4 + \mathcal{N}_{D-4}, \tag{45}$$

where $\mathcal{N}_4 = \mathcal{N}|_{D=4}$, so that $\mathcal{N}_{D-4}$ vanishes exactly in four dimensions for any value of the loop momenta. If the integral $\mathcal{I}[\mathcal{N}]$ is finite then $\mathcal{I}[\mathcal{N}_4]$ is also finite as our procedure to determine locally finite integrands could in principle be performed purely in four dimensions. Rewriting the equation above as

$$\mathcal{N}_{D-4} = \mathcal{N} - \mathcal{N}_4, \tag{46}$$

we see that as $D \to 4$ the right-hand side has to vanish and therefore $\mathcal{N}_{D-4}$ can be at most of $\mathcal{O}(\epsilon)$. To find evanescent integrands we therefore require the integrand to vanish when all loop momenta are four dimensional, that is $\mathcal{N}_4 = 0$.

For $(n > 4)$-point integrals, setting the $(D-4)$-dimensional components of each loop momentum to zero corresponds to fixing the extra components $\widehat{\ell}_i = 0$ so that all ν_{ij} vanish identically. For the numerator to vanish as $D \to 4$ we require a vanishing coefficient for every monomial of the independent scalar products $\ell_i \cdot v_{j=1,\ldots,4}$. The truncated ideal of evanescent numerators is then the intersection of the locally finite truncated ideal $\mathcal{W}$ with the one generated by the ν_{ij}.

For $(n \leq 4)$-point integrals we need to be more careful: we can still freely set to zero the coefficient of every monomial without a factor of ν_{ij}, as these are linearly independent and do not vanish as $D \to 4$. Conversely $\nu_{ij} \neq 0$ in four space-time dimensions, so evanescence of a term containing one of these factors is not guaranteed. Instead the $\widehat{\ell}_i$ become linearly dependent if enough loops are present because they span a $(5-n)$-dimensional space. As a consequence, any Gram determinant with $m \geq 6-n$ entries of the $\widehat{\ell}_i$'s will automatically vanish. For instance, with $n = 4$ we need at least two loops to find an evanescent numerator via the factor

$$G(\hat{\ell}_1 \quad \hat{\ell}_2). \tag{47}$$

This is in accordance with the fact that for the one-loop box no evanescent numerator can be extracted from Eq. (43). In general, within the space of polynomials defined by Eq. (2), the ideal of evanescent numerators for $n \leq 4$ is given by the intersection of the locally finite ideal with the ideal generated by all choices of the Gram determinant,

$$G\begin{pmatrix} \hat{\ell}_{i_1} & \cdots & \hat{\ell}_{i_{6-n}} \\ \hat{\ell}_{j_1} & \cdots & \hat{\ell}_{j_{6-n}} \end{pmatrix}. \tag{48}$$

Evanescently finite integrals. Integrands can vanish in four dimensions even if they fail the UV-finiteness power-counting criterion, or if they fail to cancel all IR divergences revealed by the Landau equations. In dimensional regularization, these combinations can give rise to *evanescently finite* integrals. These are integrals which are finite, but where the finiteness depends on cancellation of a pole in ϵ (due to a UV or IR divergence) with a factor of ϵ that arises from the evanescence properties of the integrand. Their existence is special to dimensional regularization. We will not study them exhaustively, but provide explicit examples in Sec. VII. Integrals with a cancellation of a UV divergence against evanescence arising from the IR (UV-IR evanescently finite) are expected to play a role computing rational terms in higher-loop amplitudes.

A. Massless pentagon

The massless pentagon, depicted in Fig. 4, is the simplest one-loop case where evanescent integrals arise. Let us summarize the results of our procedure applied to the pentagon. We start by writing a UV-compatible *Ansatz* for the numerator, here a rank-five polynomial in the variables,

$$\{\hat{\ell}^2, \ell \cdot v_1, \ell \cdot v_2, \ell \cdot v_3, \ell \cdot v_4\}. \tag{49}$$

This polynomial has 166 independent monomials whose coefficients are unfixed rational functions of the

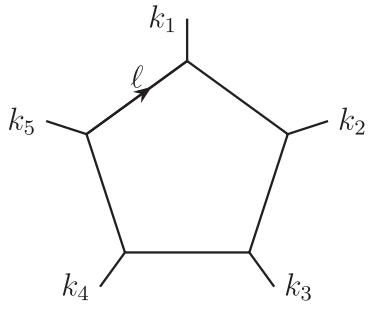

FIG. 4. Massless pentagon.

independent Mandelstam variables, for instance, the set $\{s_{12}, s_{23}, s_{34}, s_{45}, s_{51}\}$.

We proceed by listing all IR singularities. The list generalizes that for the box integral (see Table I): here we find a total of ten regions (five soft, five collinear). Requiring the numerator to vanish appropriately in each of the IR regions, we obtain a set of 141 locally finite independent numerators. The ideal needs only six generators:

$$\ell \cdot v_4 \ell \cdot (v_1 - v_2),\ (\ell - k_1) \cdot v_1 \ell \cdot (v_2 - v_3),\ \ell \cdot (v_1 - v_2) \ell \cdot (v_3 - v_4),$$
$$\ell \cdot (v_2 - v_3) \ell \cdot v_4,\ \ell \cdot (v_3 - v_4)(\ell - k_1) \cdot v_1,\ \hat{\ell}^2. \tag{50}$$

The same ideal can equivalently be expressed in terms of the closely related set of Gram determinants:

$$G\begin{pmatrix} \ell & 1 & 2 & 3 \\ \ell & 3 & 4 & 5 \end{pmatrix}, \quad G\begin{pmatrix} \ell - k_1 & 2 & 3 & 4 \\ \ell & 4 & 5 & 1 \end{pmatrix}, \quad G\begin{pmatrix} \ell & 3 & 4 & 5 \\ \ell & 5 & 1 & 2 \end{pmatrix},$$
$$G\begin{pmatrix} \ell & 4 & 5 & 1 \\ \ell & 1 & 2 & 3 \end{pmatrix}, \quad G\begin{pmatrix} \ell & 5 & 1 & 2 \\ \ell - k_1 & 2 & 3 & 4 \end{pmatrix}, \quad G(\ell \quad 1 \quad 2 \quad 3 \quad 4). \tag{51}$$

Turning to evanescent integrands, the further requirement that the numerator should vanish when the loop momenta are purely four-dimensional leads us to a subset of 40 evanescent integrals, whose numerators belong to the ideal generated by $\hat{\ell}^2 (= G(\ell \quad 1 \quad 2 \quad 3 \quad 4)/G(1 \quad 2 \quad 3 \quad 4))$, which is consistent with the well-known result,

$$\int d^D l \frac{G(\ell \quad 1 \quad 2 \quad 3 \quad 4)}{\mathcal{D}_1 \quad \cdots \quad \mathcal{D}_5} \propto (D-4) \times \int d^{D+2} l \frac{G(1 \quad 2 \quad 3 \quad 4)}{\mathcal{D}_1 \quad \cdots \quad \mathcal{D}_5} = \mathcal{O}(\epsilon). \tag{52}$$

VII. RESULTS

In this section we present some explicit results. First, we apply our procedure to characterize the locally finite integrals for the planar double box, and then show how a general conjecture for the all-loop ladder topology can be justified. We then move to consider the nonplanar double box and another two-loop four-point graph which we refer to as the beetle graph. Both the nonplanar double box and the beetle require dealing with powerlike IR singularities and allow us to illustrate aspects of our procedure.

A. Planar double box

In this section, we apply the procedures of Secs. III and IV to the massless planar double-box integral. We parametrize the loop momenta as shown in Fig. 5(a). All external momenta are outgoing and we label the edges from 1 to 7, so that their momenta read, in order of labels,

$$\ell_1,\ \ell_1 - k_1,\ \ell_1 - k_{12},\ \ell_2,\ \ell_2 - k_{123},\ \ell_2 - k_{12},\ \ell_1 - \ell_2. \tag{53}$$

We start by imposing UV-convergence constraints and then proceed to the IR analysis described in previous sections.

1. UV divergences

To avoid the overall UV divergence, the maximal allowed numerator rank is 5, in accordance with Eq. (11). Three distinct linear combinations of the loop momenta enter the denominators: ℓ_1, ℓ_2, and $(\ell_1 - \ell_2)$. Holding each one of them fixed in turn yields three possible subintegrations over the remaining variable ℓ corresponding to the dashed lines in Fig. 5(b). These give rise to the following constraints on the numerator:

$$\lim_{\rho \to \infty} \begin{cases} \rho^{-4} \mathcal{N}(\ell_1 = \text{const}, \ell_2 = \rho \ell) = 0, \\ \rho^{-4} \mathcal{N}(\ell_1 = \rho \ell, \ell_2 = \text{const}) = 0, \\ \rho^{-8} \mathcal{N}(\ell_1 = \rho \ell, \ell_2 = \text{const} + \rho \ell) = 0. \end{cases} \tag{54}$$

The first and second constraints simply count the powers of ℓ_2 and ℓ_1, respectively, so the numerator has to be at most cubic in either of the loop momenta. The third constraint is automatically satisfied for numerators of rank five. Hence, a numerator for the double box yields a UV-finite integral if it is

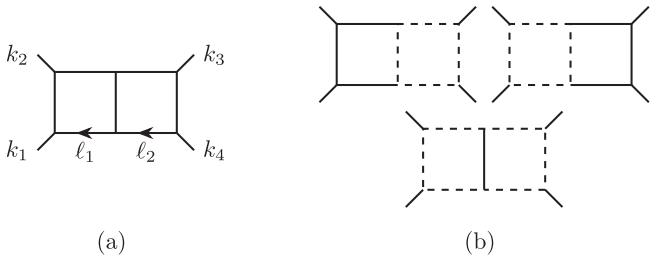

FIG. 5. The planar double-box graph (a) and and its subintegrations (b).

TABLE II. One-loop reduced diagrams of the planar double box and corresponding Symanzik polynomials.

Reduced graph	Solution of $\mathcal{U}=0$ (full graph)	Symanzik polynomials (reduced graph)
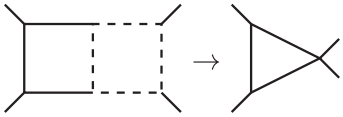	$\alpha_4=\alpha_5=\alpha_6=\alpha_7=0$	$\mathcal{U}=\alpha_1+\alpha_2+\alpha_3$ $\mathcal{F}=s\alpha_1\alpha_3$
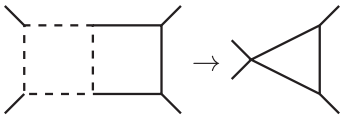	$\alpha_1=\alpha_2=\alpha_3=\alpha_7=0$	$\mathcal{U}=\alpha_4+\alpha_5+\alpha_6$ $\mathcal{F}=s\alpha_4\alpha_6$
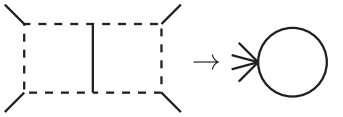	$\alpha_1=\alpha_2=\alpha_3=\alpha_4=\alpha_5=\alpha_6=0$	$\mathcal{U}=\alpha_7$ $\mathcal{F}=0$

at most cubic in ℓ_1, at most cubic in ℓ_2, and has a total rank of at most five.

2. IR divergences

Following our general algorithm of Sec. IV B, we start by identifying all reduced diagrams of the double box. We do this by computing the first Symanzik polynomial:

$$\mathcal{U}=(\alpha_1+\alpha_2+\alpha_3)(\alpha_4+\alpha_5+\alpha_6)+\alpha_7(\alpha_1+\alpha_2+\alpha_3+\alpha_4+\alpha_5+\alpha_6), \tag{55}$$

and setting $\mathcal{U}=0$ term by term. This yields three solutions which we collect in Table II. These solutions describe the reduced diagrams of Fig. 5(b). Because these diagrams already have only one loop, they represent all reduced diagrams of interest for solving the degenerate-case Landau equations: indeed, solving $\mathcal{U}=0$ monomial by monomial for the reduced diagrams gives no further solutions with at least one α_i positive.

We now have to solve the parameter-space Landau equations for the original diagram and the three reduced diagrams. We start with the planar double-box diagram itself. As the graph is planar, it is natural to express the second Symanzik polynomial $\mathcal{F}$ in terms of the independent Mandelstam invariants of consecutive external momenta, $s=(k_1+k_2)^2$ and $t=(k_2+k_3)^2$, so that $\mathcal{F}$ is subtraction free:

$$\mathcal{F}=s[\alpha_1\alpha_3(\alpha_4+\alpha_5+\alpha_6)+\alpha_4\alpha_6(\alpha_1+\alpha_2+\alpha_3)+\alpha_7(\alpha_1+\alpha_4)(\alpha_3+\alpha_6)]+t\alpha_2\alpha_5\alpha_7. \tag{56}$$

We find ten solutions of $\mathcal{F}=0$ monomial by monomial. They are listed in the first column of Table III. The last two solutions should be discarded as they nullify $\mathcal{U}$ as well. For the remaining eight solutions, we evaluate the corresponding loop momenta, recognizing the well-known double-collinear IR divergences of the planar double box. For example, the solution on the first line of Table VI gives

$$\ell_1=\frac{\alpha_2(\alpha_4+\alpha_7)}{(\alpha_1+\alpha_2)(\alpha_4+\alpha_7)+\alpha_4\alpha_7}k_1,\qquad \ell_2=\frac{\alpha_2\alpha_7}{(\alpha_1+\alpha_2)(\alpha_4+\alpha_7)+\alpha_4\alpha_7}k_1, \tag{57}$$

describing a double-collinear IR divergence $(\ell_1\parallel k_1,\ell_2\parallel k_1)$.

Computing all intersections of the surfaces associated with the singular configurations in Table II, or equivalently setting collinearity coefficients to zero or one, we reproduce the double-soft and soft-collinear IR subdivergences. For example, intersecting $(\ell_1\parallel k_1,\ell_2\parallel k_1)$ with $(\ell_1\parallel k_1,\ell_2\parallel k_4)$ gives rise to the soft-collinear configuration $(\ell_1\parallel k_1,\ell_2=0)$ as it sets $\alpha_7=0$ in Eq. (57). Similarly, intersecting $(\ell_1\parallel k_1,\ell_2\parallel k_1)$ with $(\ell_1\parallel k_4,\ell_2\parallel k_4)$ yields the double-soft divergence $(\ell_1=0,\ell_2=0)$ setting $\alpha_2=0$ in Eq. (57).

Notice that $\ell_1=0$ implies $\alpha_2\alpha_7=0$. This forbids the configuration $(\ell_1=0,\ell_2\parallel k_1)$ corresponding to a disconnected collinear diagram. More generally, the eight

TABLE III. Nondegenerate solutions of the Landau equations for the planar double box.

Solution of $\mathcal{F}=0$	Momentum constraints	
$\alpha_3=\alpha_5=\alpha_6=0$	$\ell_1\parallel k_1$	$\ell_2\parallel k_1$
$\alpha_2=\alpha_3=\alpha_6=0$	$\ell_1\parallel k_4$	$\ell_2\parallel k_4$
$\alpha_1=\alpha_4=\alpha_5=0$	$(\ell_1-k_{12})\parallel k_2$	$(\ell_2-k_{12})\parallel k_2$
$\alpha_1=\alpha_2=\alpha_4=0$	$(\ell_1-k_{12})\parallel k_3$	$(\ell_2-k_{12})\parallel k_3$
$\alpha_3=\alpha_6=\alpha_7=0$	$\ell_1\parallel k_1$	$\ell_2\parallel k_4$
$\alpha_3=\alpha_4=\alpha_7=0$	$\ell_1\parallel k_1$	$(\ell_2-k_{12})\parallel k_3$
$\alpha_1=\alpha_6=\alpha_7=0$	$(\ell_1-k_{12})\parallel k_2$	$\ell_2\parallel k_4$
$\alpha_1=\alpha_4=\alpha_7=0$	$(\ell_1-k_{12})\parallel k_2$	$(\ell_2-k_{12})\parallel k_3$
$\alpha_1=\alpha_2=\alpha_3=\alpha_7=0$	...	
$\alpha_4=\alpha_5=\alpha_6=\alpha_7=0$	...	

TABLE IV. Solutions of the Landau equations for the one-loop reduced diagrams of the planar double box.

Reduced graph	Solutions of $\mathcal{F}=0$	Momentum constraint
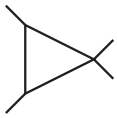	$\alpha_3=0$ $\alpha_1=0$	$\ell_1 \parallel k_1$ $(\ell_1-k_{12}) \parallel k_2$
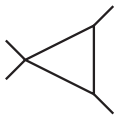	$\alpha_6=0$ $\alpha_4=0$	$\ell_2 \parallel k_4$ $(\ell_2-k_{12}) \parallel k_3$
	$\alpha_7\neq 0$	$\ell_1-\ell_2=0$

solutions of Table VI give rise to subdivergences which are in agreement with the results presented in Ref. [29].

Let us now turn to the reduced graphs of Table II. We repeat the same procedure: find all solutions of $\mathcal{F}=0$ monomial by monomial, and then compute the corresponding constraints on the loop momenta. The results of the reduced-graph analysis are given in Table IV. The first two graphs produce the familiar single-collinear divergences, as well as the single-soft divergences from intersections of solutions. The last graph gives rise to an additional single-soft configuration, which is integrable by power counting even with a trivial numerator, therefore we discard it (if we allowed higher powers of denominators, it could in principle become divergent).

As we now have the full set of singular configurations for the loop momenta, we can proceed by imposing finiteness constraints on the UV-finite numerator *Ansatz*, as described in Sec. IV C. Because all divergences (including subdivergences) are logarithmic, it suffices to require that the numerator vanishes on all collinear configurations, as in the one-loop box case. In Table V we list the numbers of linearly independent finite and evanescent $[\mathcal{O}(\epsilon)]$ integrals up to a given rank, along with the number of the corresponding generators arising at each rank. We construct them in the next section.

TABLE V. Results of the double-box numerator analysis. The counts for the integrals are inclusive of lower ranks, while the counts for generators are not.

Rank	1	2	3	4	5
Number of finite integrals	0	2	18	89	247
Number of new finite generators	0	2	4	4	0
Number of evanescent integrals	0	0	0	1	7
Number of new evanescent generators	0	0	0	1	0

3. Finding a basis of generators

Thus far, we have identified the truncated ideals corresponding to locally finite and evanescent numerators for the double-box integral. We now turn to finding a compact and nice representation for the generators of these ideals. To do so, we start by defining[9] the rank-one monomials,

$$\begin{aligned}&\beta_1=\ell_1\cdot v_2, \quad \beta_2=(\ell_1-k_{12})\cdot v_1,\\ &\beta_3=(\ell_2-k_{12})\cdot v_2, \qquad \beta_4=\ell_2\cdot(v_2-v_3),\\ &\beta_{12}=\ell_1\cdot v_3, \quad \beta_{34}=(\ell_2-k_{123})\cdot(v_1-v_2).\end{aligned} \tag{58}$$

These turn out to have simple representations in terms of Gram determinants (see Appendix A 1). The β_i variables are rank-one numerators which vanish in the collinear region associated to the k_i; the β_{ij} are rank one which vanish in the collinear regions associated to both k_i and k_j. In addition, $\beta_1\beta_2$ and β_{12} vanish in all soft limits involving ℓ_1; by symmetry, $\beta_3\beta_4$ and β_{34} vanish in those involving ℓ_2.

Thanks to their properties we can use the βs together with the ν_{ij} as building blocks for the basis of the ideal of locally finite numerators for the double box. We write down the simplest combinations that cancel all divergences, making sure not to repeat any lower rank basis element when writing higher rank ones. Starting at rank two, we find that only the combinations $\beta_{12}\beta_{34}$ and ν_{12} are locally finite. In fact, they correspond to the desired rank-two generators. At rank three we have more options. For instance, we can tame the singularities associated with legs 1 and 2 using two different βs, and the ones of legs 3 and 4 with a single one: $\beta_1\beta_2\beta_{34}$. By symmetry we can also choose $\beta_{12}\beta_3\beta_4$. In addition, because the $\widehat{\ell}_i$ vanish in any IR limit, we can write down two more rank-three generators, $\nu_{11}\beta_{34}$ and $\nu_{22}\beta_{12}$. Finally, at rank four we have the following options:

(1) cancel the divergence on each corner separately using the product $\beta_1\beta_2\beta_3\beta_4$;
(2) use β_1 and β_2 to remove the singularities associated with ℓ_1, and ν_{22} to remove those of ℓ_2, using the product $\beta_1\beta_2\nu_{22}$;
(3) use the flipped version $\beta_3\beta_4\nu_{11}$; and
(4) use only the $\hat{\ell}$ components of the loop momenta, with the product $\nu_{11}\nu_{22}$.

Together, these options give us all four rank-four generators. Summarizing, we find the double-box generators,

[9]These definitions depend both on the loop-momentum routing and the choice made for momentum conservation ($k_4=-k_1-k_2-k_3$ in our case). Any changes will be reflected on the explicit form of the βs.

$$\begin{aligned}&\text{rank two: } \beta_{12}\beta_{34}, \quad \nu_{12},\\ &\text{rank three: } \beta_1\beta_2\beta_{34}, \quad \beta_{12}\beta_3\beta_4, \quad \nu_{11}\beta_{34}, \quad \nu_{22}\beta_{12},\\ &\text{rank four: } \beta_1\beta_2\beta_3\beta_4, \quad \nu_{11}\beta_3\beta_4, \quad \nu_{22}\beta_1\beta_2, \quad \nu_{11}\nu_{22}.\end{aligned} \tag{59}$$

Using computational algebraic geometry, we have checked that this set of generators is nonredundant and indeed generates the entire truncated ideal of locally finite numerators.

Because we have only three independent external momenta, we can look to Gram determinants built out of the $\hat{\ell}$ components of the available loop momenta to build evanescent generators [$\mathcal{O}(\epsilon)$]. At two loops the only possible combination is

$$G(\hat{\ell}_1 \quad \hat{\ell}_2) = \nu_{11}\nu_{22} - \nu_{12}^2 \propto G(\ell_1 \quad \ell_2 \quad k_1 \quad k_2 \quad k_3). \tag{60}$$

This is indeed the only evanescent generator, as can be seen from the counting in Table V. The evanescent ideal is then generated by

$$\nu_{11}\nu_{22} - \nu_{12}^2. \tag{61}$$

Every evanescent numerator is by definition also locally finite, and this generator can be written in terms of the generators in Eq. (59). In order to make the subset of evanescent numerators more manifest within the locally finite ones, we could alternatively choose the rank-four generators for the planar double box to be

$$\beta_1\beta_2\beta_3\beta_4, \quad \nu_{11}\beta_3\beta_4, \quad \nu_{22}\beta_1\beta_2, \quad \nu_{11}\nu_{22} - \nu_{12}^2. \tag{62}$$

Beyond evanescence, we can also form combinations of locally finite integrands that for symmetry reasons give rise to identically vanishing integrals (i.e., to all orders in ϵ). We will not discuss these any further. We also leave the question of combining local finiteness with integration-by-parts reduction to future investigation.

We can obtain examples of evanescently finite integrands for the planar double box within the evanescent ideal by selecting UV-divergent numerators such as $(\nu_{11}\nu_{22} - \nu_{12}^2)\,\ell_1\cdot\ell_2$ or $(\nu_{11}\nu_{22} - \nu_{12}^2)\,\ell_1\cdot k_1\,\ell_2\cdot k_2$.

B. Ladder integrals: An all-loop conjecture

Assuming that all integrals with ladder topologies have singularities that are at worst logarithmic in the IR (as is plausible), the reasoning in the previous section can be extended directly to all loop orders. In order to do so, we generalize Eq. (58),

$$\begin{aligned}&\beta_1 = \ell_1\cdot v_2,\ \beta_2 = (\ell_1 - k_{12})\cdot v_1,\ \beta_3 = (\ell_L - k_{12})\cdot v_2,\ \beta_4 = \ell_L\cdot(v_2 - v_3),\\ &\beta_{12} = \ell_1\cdot v_3,\ \beta_{34} = (\ell_L - k_{123})\cdot(v_1 - v_2).\end{aligned} \tag{63}$$

Using these variables and defining the L-loop momenta as in Fig. 6, our conjecture for the generators of the truncated ideal of locally finite numerators takes the remarkably simple form,

$$\begin{aligned}&\text{rank two: } \beta_{12}\beta_{34},\ \nu_{1,L},\\ &\text{rank three: } \beta_1\beta_2\beta_{34},\ \beta_{12}\beta_3\beta_4,\ \nu_{1,i\neq L}\beta_{34},\ \nu_{L,i\neq 1}\beta_{12},\\ &\text{rank four: } \beta_1\beta_2\beta_3\beta_4,\ \nu_{1,i\neq L}\beta_3\beta_4,\ \nu_{L,i\neq 1}\beta_1\beta_2, \qquad \nu_{1,i\neq L}\nu_{L,j\neq 1}.\end{aligned} \tag{64}$$

We thus have two conjectured generators at rank two, $2L$ generators at rank three, L^2 generators at rank four, with no additional generators beyond rank four. The larger number of generators is simply due to having more loop momenta at our disposal to build some of the ν_{ij} combinations. The role of the scattering-plane variables β is unchanged.

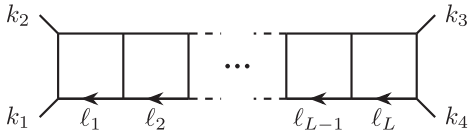

FIG. 6. All-loop ladder integral.

As to evanescent generators, we see that (see Sec. VI) every Gram determinant involving at least two different $\widehat{\ell}_i$ will automatically vanish as $D \to 4$. It follows that the truncated ideal of evanescent numerators is the intersection of the locally finite one of Eq. (64) with the one generated by the two-by-two Gram determinants,

$$G\begin{pmatrix}\hat{\ell}_{i_1} & \hat{\ell}_{i_2}\\ \hat{\ell}_{j_1} & \hat{\ell}_{j_2}\end{pmatrix} = \nu_{i_1 j_1}\nu_{i_2 j_2} - \nu_{i_1 j_2}\nu_{i_2 j_1}. \tag{65}$$

We can write out the intersection explicitly, finding that it is generated by the set,

$$\begin{aligned}
&\text{rank four:}\ \nu_{1i}\nu_{Lj}-\nu_{1j}\nu_{Li}, \qquad \nu_{1L}\nu_{k_1h_1}-\nu_{1h_1}\nu_{k_1L},\\
&\text{rank five:}\ (\nu_{1k_1}\nu_{k_3k_2}-\nu_{1k_2}\nu_{k_3k_1})\beta_{34}, \qquad (\nu_{Lh_1}\nu_{h_3h_2}-\nu_{Lh_2}\nu_{h_3h_1})\beta_{12},\\
&\text{rank six:}\ (\nu_{1k_1}\nu_{k_3k_2}-\nu_{1k_2}\nu_{k_3k_1})\beta_3\beta_4, \qquad (\nu_{Lh_1}\nu_{h_3h_2}-\nu_{Lh_2}\nu_{h_3h_1})\beta_1\beta_2,\\
&\qquad (\nu_{l_1l_3}\nu_{l_2l_4}-\nu_{l_1l_4}\nu_{l_2l_3})\beta_{12}\beta_{34},\\
&\text{rank seven:}\ (\nu_{l_1l_3}\nu_{l_2l_4}-\nu_{l_1l_4}\nu_{l_2l_3})\beta_{12}\beta_3\beta_4, \qquad (\nu_{l_1l_3}\nu_{l_2l_4}-\nu_{l_1l_4}\nu_{l_2l_3})\beta_1\beta_2\beta_{34},\\
&\text{rank eight:}\ (\nu_{l_1l_3}\nu_{l_2l_4}-\nu_{l_1l_4}\nu_{l_2l_3})\beta_1\beta_2\beta_3\beta_4,
\end{aligned} \tag{66}$$

where the indices are defined as

$$i,j=1,\ldots,L, \qquad k_r=1,\ldots,L-1, \qquad h_r=2,\ldots,L, \qquad l_r=2,\ldots,L-1, \tag{67}$$

in order to avoid double counting of lower-rank generators and are assumed to take values for which the corresponding generator is nonzero, e.g., the choice $l_1=l_2=l_3=l_4=2$ is forbidden because most generators at ranks six, seven, and eight would vanish identically. The evanescent generators above can be written in terms of the locally finite generators in Eq. (64). From Eq. (66) we find the following numbers of generators at each rank:

$$\begin{aligned}
&\text{rank four:}\ (3L^2-9L+8)/2,\\
&\text{rank five:}\ (L-2)(L^2-4L+5),\\
&\text{rank six:}\ (L-2)(L^3-9L+16)/8,\\
&\text{rank seven:}\ (L-2)(L-3)(L^2-5L+8)/4,\\
&\text{rank eight:}\ (L-2)(L-3)(L^2-5L+8)/8.
\end{aligned} \tag{68}$$

We deduce that the rank-four generators are present for any number of loops, while those at ranks five and six require a minimum of three loops, and those at ranks seven and eight first appear at four loops. All locally finite and evanescent generators in Eqs. (64) and (66) are UV finite.

We have verified the validity of this conjecture at two, three, and four loops by explicit computation of the ideals.

C. Nonplanar double box

We next consider the nonplanar double-box integral. There are two important differences between the planar and nonplanar double box integrals. In particular, the nonplanar one:

(1) lacks a subtraction-free form (see Sec. IV B) for the $\mathcal{F}$ polynomial; and
(2) has powerlike soft divergences: regions of the loop integration where the integrand scales as $\mathrm{d}\lambda\,\lambda^{-\alpha}$ with $\alpha>1$.

For these reasons we believe the nonplanar box to be an instructive example. We repeat the procedure outlined in the previous section, highlighting the role of powerlike divergences along the way.

The loop momenta are parametrized as shown in Fig. 7(a) with all external momenta outgoing and we label the edges from 1 to 7 so that their momenta read, in increasing order of labels,

$$\begin{aligned}
&\ell_1,\ \ell_1-k_1,\ \ell_1-k_{12},\ \ell_2,\\
&\ell_2-k_{123},\ \ell_2-\ell_1-k_3,\ \ell_1-\ell_2.
\end{aligned} \tag{69}$$

As before, we start by imposing UV-convergence constraints and proceed to the IR analysis afterwards.

1. UV divergences

The maximal allowed numerator rank is five and there are three distinct subintegrations corresponding to the dashed lines in Fig. 7(b). These give rise to the following constraints on the numerator:

$$\lim_{\rho\to\infty}\begin{cases}\rho^{-4}\mathcal{N}(\ell_1=\text{const},\ell_2=\rho\ell)=0,\\ \rho^{-6}\mathcal{N}(\ell_1=\rho\ell,\ell_2=\text{const})=0,\\ \rho^{-6}\mathcal{N}(\ell_1=\rho\ell,\ell_2=\text{const}+\rho\ell)=0.\end{cases} \tag{70}$$

Overall, a UV-finite numerator for the nonplanar double box should be at most of rank five, with maximum degrees of five and three in ℓ_1 and ℓ_2, respectively.

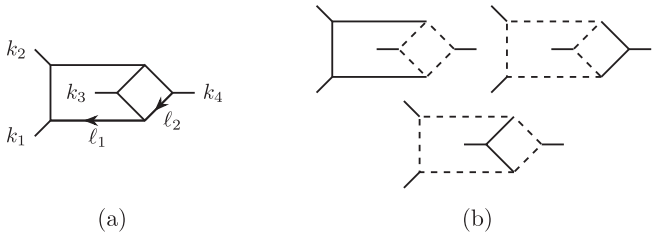

FIG. 7. The nonplanar double-box graph (a) and its subintegrations (b).

2. IR divergences

As before, the relevant reduced diagrams correspond to the zeros of the first Symanzik polynomial:

$$\mathcal{U} = (\alpha_1 + \alpha_2 + \alpha_3)(\alpha_4 + \alpha_5 + \alpha_6 + \alpha_7) + (\alpha_4 + \alpha_5)(\alpha_6 + \alpha_7), \tag{71}$$

and reproduce the subintegrations of Fig. 7(b). To solve the parameter-space Landau equations for the full diagram, we compute the second Symanzik polynomial:

$$\mathcal{F} = s[\alpha_1\alpha_3(\alpha_4 + \alpha_5 + \alpha_6 + \alpha_7) + \alpha_1\alpha_5\alpha_6 + \alpha_3\alpha_4\alpha_7] + t\alpha_2\alpha_5\alpha_7 - (s+t)\alpha_2\alpha_4\alpha_6. \tag{72}$$

Unlike the planar case, $\mathcal{F}$ is no longer a sum of positive terms for appropriate signs of the Mandelstam invariants. Therefore, we consider instead the most general linear combination of the Landau equations (25),

$$\begin{aligned}\sum_{e=1}^{E} w_e\alpha_e\frac{\partial}{\partial\alpha_e}\mathcal{F} = {} & s(w_1 + w_3 + w_4)\alpha_1\alpha_3\alpha_4 + s(w_1 + w_3 + w_5)\alpha_1\alpha_3\alpha_5 \\ & + s(w_1 + w_3 + w_6)\alpha_1\alpha_3\alpha_6 + s(w_1 + w_3 + w_7)\alpha_1\alpha_3\alpha_7 \\ & + s(w_1 + w_5 + w_6)\alpha_1\alpha_5\alpha_6 + s(w_3 + w_4 + w_7)\alpha_3\alpha_4\alpha_7 \\ & + t(w_2 + w_5 + w_7)\alpha_2\alpha_5\alpha_7 - (s+t)(w_2 + w_4 + w_6)\alpha_2\alpha_4\alpha_6,\end{aligned} \tag{73}$$

and require that each coefficient is strictly positive when $s, t > 0$. It is straightforward to check that the resulting system of linear inequalities is feasible: one possible solution is

$$\vec{w} = (0, -1, 1, 0, 2, 0, 0). \tag{74}$$

This means that a subtraction-free linear combination of the Landau equations exists, therefore we can find their solutions simply by setting $\mathcal{F}$ to zero term by term as usual; in other words, no divergences due to cancellations in $\mathcal{F}$ can occur (see also Appendix A of Ref. [44]). For the reduced diagrams, $\mathcal{F}$ is subtraction free itself, so their analysis does not pose any difficulty.

Solutions of the Landau equations correspond to double- and single-collinear IR divergences, all of which are logarithmic. However, if we take intersections of these solutions we find additional subdivergences, two of which are powerlike. These are the double-soft configurations $(\ell_1 = 0, \ell_2 = 0)$ and $(\ell_1 = k_1 + k_2, \ell_2 = -k_4)$, in accordance with Ref. [29]. Therefore, unlike the planar case, cancellation of collinear configurations alone is insufficient. In principle, one has to expand the UV-finite *Ansatz* to a certain subleading order in the vicinity of the powerlike configurations, and require that these divergent contributions vanish. In practice, however, we find that these additional constraints are satisfied automatically as long as all collinear divergences are canceled. We report the results of our analysis in Table VI.

TABLE VI. Results of the nonplanar double-box numerator analysis. The counts for the integrals are inclusive of lower ranks, while the counts for generators are not.

Rank	1	2	3	4	5
Number of finite integrals	0	0	9	65	230
Number of new finite generators	0	0	9	8	0
Number of evanescent integrals	0	0	0	1	7
Number of new evanescent generators	0	0	0	1	0

3. Finding a basis of generators

By analogy with the planar double box we can define a set of variables,

$$\begin{aligned}&\beta_1 = \ell_1 \cdot v_2, \quad \beta_2 = (\ell_1 - k_{12}) \cdot v_1, \quad \beta_3 = (\ell_1 - \ell_2) \cdot v_1, \\ &\beta_3' = (\ell_1 - \ell_2) \cdot v_2, \quad \beta_4 = \ell_2 \cdot (v_1 - v_2), \\ &\beta_4' = \ell_2 \cdot (v_2 - v_3), \quad \beta_{12} = \ell_1 \cdot v_3,\end{aligned} \tag{75}$$

which vanish on appropriate collinear and soft limits. In particular, each β_S (and β_S') vanishes on the collinear configurations involving the particles in S, and also vanishes on the soft limits involving the combinations of loop momenta in its definition. In terms of these quantities we find the generators:

$$\begin{aligned}
&\text{rank three: } \beta_{12}\beta_3\beta_4,\ \beta_{12}\beta_3'\beta_4,\ \beta_{12}\beta_3\beta_4',\ \beta_{12}\beta_3'\beta_4',\ \beta_{12}(\nu_{12}-\nu_{22}),\\
&\qquad \beta_3\nu_{12},\ \beta_3'\nu_{12},\ \beta_4(\nu_{11}-\nu_{12}),\ \beta_4'(\nu_{11}-\nu_{12}),\\
&\text{rank four: } \beta_1\beta_2\beta_3\beta_4,\ \beta_1\beta_2\beta_3'\beta_4,\ \beta_1\beta_2\beta_3\beta_4',\ \beta_1\beta_2\beta_3'\beta_4',\\
&\qquad \beta_1\beta_2(\nu_{12}-\nu_{22}),\ \nu_{12}(\nu_{11}-\nu_{12}),\ \nu_{12}(\nu_{12}-\nu_{22}),\ \nu_{11}\nu_{22}-\nu_{12}^2.
\end{aligned} \tag{76}$$

Just as for the planar double box, we have only three independent external and two loop momenta, so we expect a single evanescent generator. This is indeed the case: it is $G(\hat{\ell}_1\ \hat{\ell}_2) = \nu_{11}\nu_{22} - \nu_{12}^2$.

D. Two-loop beetle

In this section we briefly treat the "beetle" integral of Fig. 8(a). We will not show the whole procedure here, but simply provide results for the locally finite and evanescent truncated ideals.

This integral is of interest to us because it contains powerlike double-collinear [see Fig. 8(b)] and soft-collinear divergences, which did not appear in any of the cases treated above. The presence of powerlike divergences involving collinear configurations requires us to take into account Eq. (31) for the first time in this article. In practice, as we will see shortly, this introduces a dependence on the Mandelstam variables s_{ij} in the set of generators for the ideal of locally finite numerators. To describe our results, we can define the set of rank-one monomials,

$$\begin{aligned}
&\beta_1 = \ell_1\cdot v_2, \qquad \beta_{12} = \ell_1\cdot v_3, \qquad \gamma_1 = \ell_2\cdot v_2, \qquad \gamma_3 = (\ell_2 - k_{12})\cdot v_2,\\
&\gamma_{12} = \ell_2\cdot v_3, \qquad \gamma_{14} = \ell_2\cdot(v_2 - v_3), \qquad \gamma_{34} = \ell_2\cdot(v_1 - v_2), \qquad \gamma_{23} = (\ell_2 - k_1)\cdot v_1,
\end{aligned} \tag{77}$$

so that the β_S (respectively, the γ_S) vanish on collinear configurations of ℓ_1 (respectively, ℓ_2) involving the external momenta in S. In terms of these variables,[10] we can express the set of generators as follows:

$$\begin{aligned}
&\text{rank three: } \gamma_{12}\gamma_{34}(s_{12}\beta_1 + s_{13}\beta_{12}), \qquad \gamma_{14}\gamma_{23}(s_{12}\beta_1 + s_{13}\beta_{12}),\\
&\qquad \beta_1\nu_{22}, \qquad \beta_{12}\nu_{22}, \qquad \gamma_1\nu_{12}, \qquad \gamma_{12}\nu_{12},\\
&\text{rank four: } \beta_1\gamma_{12}\gamma_{34}(s_{12}\gamma_1 + s_{13}\gamma_{12}), \qquad \beta_1\gamma_{14}\gamma_{23}(s_{12}\gamma_1 + s_{13}\gamma_{12}),\\
&\qquad \beta_{12}\gamma_{12}^2\gamma_{34}, \qquad \beta_{12}\gamma_{12}\gamma_{23}\gamma_{14},\\
&\qquad \beta_1\gamma_{23}[s_{23}\gamma_1^2 + (\gamma_1+\gamma_{34})(s_{12}\gamma_1 + s_{13}\gamma_{12})], \qquad \nu_{12}\nu_{22}.
\end{aligned} \tag{78}$$

The polynomial $\beta_1 s_{12} + \beta_{12} s_{13}$ and its equivalent with $\beta \to \gamma$ are related to standard scalar products of loop and external momenta,

$$\beta_1 s_{12} + \beta_{12} s_{13} = 2k_1\cdot\ell_1 \quad \text{and} \quad \gamma_1 s_{12} + \gamma_{12} s_{13} = 2k_1\cdot\ell_2. \tag{79}$$

Finally we find that, within the UV power counting, there are no evanescent numerators for the beetle integral.

E. Two-loop four-gluon helicity amplitudes

In this section, we present a simple but concrete application of the concepts and results discussed in previous sections. We focus on the leading-color amplitudes for two-loop scattering of four gluons in pure

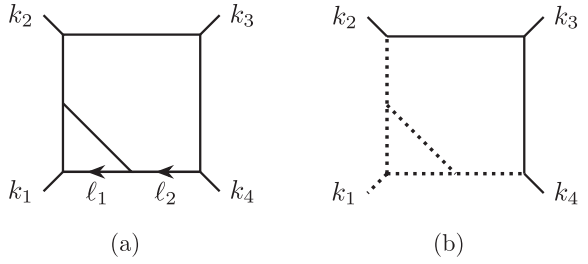

FIG. 8. The beetle graph (a) and a collinear configuration leading to a powerlike divergence (b). In (b) teal dotted edges are collinear to k_1.

[10]The variables in Eq. (77) are not all linearly independent. We express our results in terms of an overcomplete set for the sake of clarity.

Yang-Mills theory. Very compact expressions for the all-plus amplitude have been known for a long time [53] and expressions for all other helicity configurations were first computed in Refs. [54,55]. Our goal here is not to obtain the most compact results, but rather to give a hint of how using locally finite integrals allows us to shift IR divergences out of the top-level topology. This offers a simpler representation, where the overall divergence is more manifest. For our example, we make use of the rank-two locally finite numerators of Eq. (59),

$$f_1(k_1,k_2,k_3,k_4)=\beta_{12}\beta_{34}, \qquad f_2(k_1,k_2,k_3,k_4)=\nu_{12}, \tag{80}$$

to write the bare four-gluon helicity amplitudes in a basis of 13 master integrals as follows:

$$\mathcal{A}^{0\to gggg}(\boldsymbol{\lambda}) = \Big[r_1^{\boldsymbol{\lambda}} \,[f_1(k_1,k_2,k_3,k_4)] + r_2^{\boldsymbol{\lambda}} \,[f_2(k_1,k_2,k_3,k_4)] + r_3^{\boldsymbol{\lambda}} \,[f_1(k_4,k_1,k_2,k_3)] + r_4^{\boldsymbol{\lambda}} \,[f_2(k_4,k_1,k_2,k_3)] + r_5^{\boldsymbol{\lambda}} + r_6^{\boldsymbol{\lambda}} + r_7^{\boldsymbol{\lambda}} + r_8^{\boldsymbol{\lambda}} + r_9^{\boldsymbol{\lambda}} + r_{10}^{\boldsymbol{\lambda}} + r_{11}^{\boldsymbol{\lambda}} + r_{12}^{\boldsymbol{\lambda}} + r_{13}^{\boldsymbol{\lambda}} \Big] \Phi(\boldsymbol{\lambda})\,. \tag{81}$$

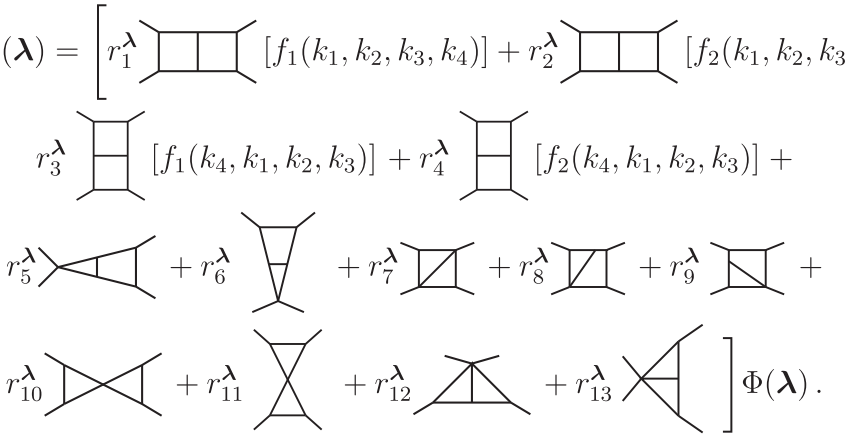

Here, $\mathcal{A}^{0\to gggg}(\boldsymbol{\lambda})$ is the coefficient of the color factor $N_c^2\,\mathrm{Tr}[T^{a_1}T^{a_2}T^{a_3}T^{a_4}]$ for the helicity configuration $\boldsymbol{\lambda}=\{\lambda_1,\lambda_2,\lambda_3,\lambda_4\}$ (N_c is the dimension of the Yang-Mills group and a_i is the color index of the ith gluon). The coefficients $r_i^{\boldsymbol{\lambda}}$ are rational functions of the space-time dimensions D and of the independent Mandelstam variables s_{12}, s_{23}. Finally, $\Phi(\boldsymbol{\lambda})$ is an overall spinor factor.

The first four integrals in Eq. (81) are locally finite, and contain the whole dependence on the double-box topology (the one with the largest number of propagators). The numerators of Eq. (80) correspond to linear combinations of the chiral numerators presented in Ref. [56]. The remaining nine integrals are chosen to match as closely as possible the IR singularities obtained from the Landau equations. Because our analysis is for the moment limited to IR-finite integrals, we do not have a systematic way to select IR-divergent integrals. We postpone an investigation of this aspect to future work.

With the choice of master integrals adopted in Eq. (81), we observe that all rational coefficients $r_i^{\boldsymbol{\lambda}}$ are regular in the limit $\epsilon\to 0$, implying that all divergences are contained in the integrals themselves.

The helicity configurations which vanish at tree level have an overall factor of ϵ so that, so long as we are interested in the amplitudes only up to $\mathcal{O}(\epsilon^0)$, we can safely drop all locally finite integrals. We then find

$$\mathcal{A}^{0\to gggg}(+,+,+,+) = \epsilon\, C(\epsilon) \Big[\tilde{r}_5 + \tilde{r}_6 + \tilde{r}_7 + \tilde{r}_8 + \tilde{r}_9 + \tilde{r}_{10} + \tilde{r}_{11} + \tilde{r}_{12} + \tilde{r}_{13} \Big] \Phi(+,+,+,+)\,, \tag{82}$$

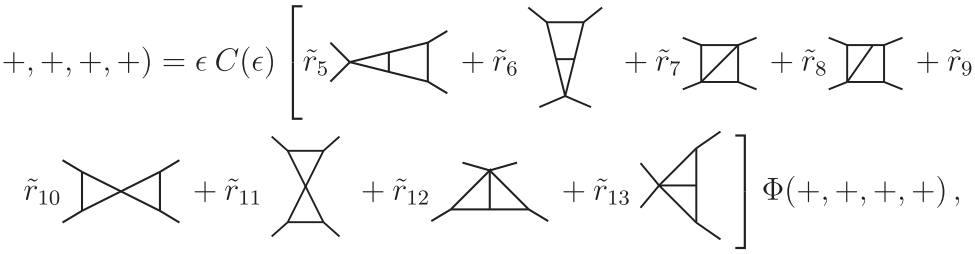

where we have defined the rational coefficients $\tilde{r}_i$ to make the overall factor of ϵ explicit, and where the ϵ-dependent coefficient $C(\epsilon)$ approaches a finite constant as $\epsilon\to 0$. We collect the explicit expressions for the coefficients in Appendix B. A similar expression holds for the single-minus amplitude. Our choice of master integrals makes Eq. (82) free of contributions related to the double box, the most complicated topology for this process.

VIII. CONCLUSIONS

In this article, we presented a systematic approach to finding locally finite integrands for Feynman integrals. Such integrands yield integrals which are UV and IR finite, and which are integrable everywhere in loop-momentum space. They can be evaluated in four dimensions. The locally IR-finite integrands form an ideal, which we can truncate to a finite-dimensional space of UV-finite integrands. We showed how to write the generators of the ideal in a compact form using either dual vectors or Gram determinants.

We also presented the class of evanescent integrands, a subset of locally finite ones. These integrands give rise to integrals which are of $\mathcal{O}(\epsilon)$ in the dimensional regulator, and so will vanish in the four-dimensional limit. They can give rise to new identities between Feynman integrals. We also briefly discussed evanescently finite integrands. These give rise to finite integrals whose finiteness arises from cancellation of a UV or IR divergence with a factor of ϵ arising from the integration. Such integrands are special to dimensional regularization, but may play a role in providing expressions for rational terms beyond one loop. We leave a more thorough investigation of such integrands to future work.

We presented several explicit examples at two loops: the planar and nonplanar double boxes, as well as the integral of Fig. 8. We also presented a conjecture for the locally finite and evanescent integrands for all ladder integrals. We verified the conjecture at three and four loops. Both classes of integrands will be pruned through use of integration-by-parts (IBP) identities [3,4], though ideally these would be applied in a way that respects finiteness or evanescence. We believe a compatible approach is possible and an interesting subject for investigation.

The isolation of locally finite and evanescent integrands represents the first step in a program of reorganizing integrands in classes of uniform UV and IR divergence. A next step, for example, could be isolating all integrals with $1/\epsilon$ divergences of IR origin. We illustrated the promise of such a reorganization by showing that the expressions for planar two-loop four-gluon amplitudes simplify considerably when we make use of finite integrals as master integrals.

The interplay between finite or evanescent integrands and the class of so-called local integrands [5] also offers an interesting subject for investigation. The local integrands allow one to express scattering amplitudes in a manifestly local form. In addition, they give rise to integrals with especially simple analytic properties. The integrals fulfil simple differential equations, and can be expressed as pure combinations of functions of uniform transcendental weight [7]. The algorithms presented in this paper, in combination with a suitable set of IBP identities as described above, offer an opportunity to investigate these classes of integrals from a more general perspective.

ACKNOWLEDGMENTS

We thank Michael Borinsky, Leonardo de la Cruz, Andreas von Manteuffel, Ben Page, Stefan Weinzierl, and Yang Zhang for helpful discussions. This work was supported in part by the Excellence Cluster ORIGINS funded by the Deutsche Forschungsgemeinschaft (DFG, German Research Foundation) under Germany's Excellence Strategy—EXC–2094–390783311, by the European Research Council (ERC) under the European Union's research and innovation program Grant Agreements No. ERC–AdG–885414 ("Ampl2Einstein") and No. ERC–StG–949279 ("HighPHun"), by the Royal Society under the Royal Society University Research Fellowship (URF/R1/191125), and by the National Science Foundation under Grant No. NSF PHY-1748958 to the Kavli Institute for Theoretical Physics (KITP).

APPENDIX A: GRAM DETERMINANT REPRESENTATION FOR LOCALLY FINITE NUMERATORS

In this section we present examples of Gram-determinant representations for the truncated ideals of locally finite numerators.

1. Double box

We found that Eq. (59) is a complete basis of locally finite numerators for the double-box topology. An equivalent basis can be obtained in terms of Gram determinants and reads

$$\begin{aligned}
&\text{rank two: } G\begin{pmatrix} \ell_1\,1\,2 \\ \ell_2\,3\,4 \end{pmatrix}, \qquad G\begin{pmatrix} \ell_1\,1\,2\,3 \\ \ell_2\,1\,2\,3 \end{pmatrix}, \\
&\text{rank three: } G(\ell_2\,3\,4)G\begin{pmatrix} \ell_1\,1\,2 \\ 1\,2\,4 \end{pmatrix}, \qquad G(\ell_1\,1\,2)G\begin{pmatrix} \ell_2\,3\,4 \\ 1\,2\,4 \end{pmatrix}, \\
&\qquad (\ell_2+k_4)^2 G\begin{pmatrix} \ell_1\,1\,2 \\ 1\,2\,4 \end{pmatrix}, \qquad (\ell_1-k_1)^2 G\begin{pmatrix} \ell_2\,3\,4 \\ 1\,2\,4 \end{pmatrix} \\
&\text{rank four: } (\ell_2+k_4)^2 G(\ell_1\,1\,2), \qquad (\ell_1-k_1)^2 G(\ell_2\,3\,4), \\
&\qquad (\ell_1-k_1)^2(\ell_2+k_4)^2,\ G(\ell_1\ell_2 123).
\end{aligned} \tag{A1}$$

The lone rank-four evanescent generator of Eq. (61) corresponds to the Gram determinant,

$$G(\ell_1\ \ell_2\ 1\ 2\ 3). \tag{A2}$$

The basis in Eq. (A1) is not unique; in general, one can take linear combinations of the generators to construct different bases. For example, an alternative choice for the rank-two generators is

$$G\begin{pmatrix}\ell_1\ 1\ 2\\ \ell_2\ 3\ 4\end{pmatrix},\qquad G\begin{pmatrix}\ell_1\ 1\ 2\\ 1\ 2\ 3\end{pmatrix}G\begin{pmatrix}\ell_2\ 3\ 4\\ 1\ 2\ 3\end{pmatrix}. \tag{A3}$$

2. Nonplanar double box

One possible choice of Gram-determinant representation for the locally finite basis of Eq. (76) is

$$\begin{aligned}
\text{rank three:}\ & G\begin{pmatrix}\ell_1\ 1\ 2\\ 1\ 2\ 3\end{pmatrix}G\begin{pmatrix}\ell_2\ 4\\ 1\ 2\end{pmatrix}G\begin{pmatrix}\ell_1-\ell_2\ 3\\ 1\quad 2\end{pmatrix},\qquad G\begin{pmatrix}\ell_1\ 1\ 2\\ 1\ 2\ 3\end{pmatrix}G\begin{pmatrix}\ell_2\ 4\\ 2\ 3\end{pmatrix}G\begin{pmatrix}\ell_1-\ell_2\ 3\\ 2\quad 3\end{pmatrix},\\
& G\begin{pmatrix}\ell_1\ 1\ 2\\ 1\ 2\ 3\end{pmatrix}G\begin{pmatrix}\ell_2\ 4\\ 3\ 4\end{pmatrix}G\begin{pmatrix}\ell_1-\ell_2\ 3\\ 3\quad 4\end{pmatrix},\qquad G\begin{pmatrix}\ell_1\ 1\ 2\\ 1\ 2\ 3\end{pmatrix}G\begin{pmatrix}\ell_2\ 4\\ 4\ 1\end{pmatrix}G\begin{pmatrix}\ell_1-\ell_2\ 3\\ 4\quad 1\end{pmatrix},\\
& G\begin{pmatrix}\ell_2\quad 4\\ \ell_1-\ell_2\ 3\end{pmatrix}G\begin{pmatrix}\ell_1\ 1\ 2\\ 1\ 2\ 3\end{pmatrix},\qquad G\begin{pmatrix}\ell_2\ 4\\ 1\ 2\end{pmatrix}G\begin{pmatrix}\ell_1\quad 1\quad 2\\ \ell_1-\ell_2\ 3\ 1\end{pmatrix},\\
& G\begin{pmatrix}\ell_2\ 4\\ 2\ 3\end{pmatrix}G\begin{pmatrix}\ell_1\quad 1\quad 2\\ \ell_1-\ell_2\ 3\ 1\end{pmatrix},\qquad G\begin{pmatrix}\ell_1-\ell_2\ 3\\ 1\quad 2\end{pmatrix}G\begin{pmatrix}\ell_1\ 1\ 2\\ \ell_2\ 4\ 1\end{pmatrix},\\
& G\begin{pmatrix}\ell_1-\ell_2\ 3\\ 2\quad 3\end{pmatrix}G\begin{pmatrix}\ell_1\ 1\ 2\\ \ell_2\ 4\ 1\end{pmatrix},\\
\text{rank four:}\ & (\ell_1-k_1)^2G\begin{pmatrix}\ell_2\ 4\\ 1\ 2\end{pmatrix}G\begin{pmatrix}\ell_1-\ell_2\ 3\\ 1\quad 2\end{pmatrix},\qquad (\ell_1-k_1)^2G\begin{pmatrix}\ell_2\ 4\\ 2\ 3\end{pmatrix}G\begin{pmatrix}\ell_1-\ell_2\ 3\\ 2\quad 3\end{pmatrix},\\
& (\ell_1-k_1)^2G\begin{pmatrix}\ell_2\ 4\\ 3\ 4\end{pmatrix}G\begin{pmatrix}\ell_1-\ell_2\ 3\\ 3\quad 4\end{pmatrix},\qquad (\ell_1-k_1)^2G\begin{pmatrix}\ell_2\ 4\\ 4\ 1\end{pmatrix}G\begin{pmatrix}\ell_1-\ell_2\ 3\\ 4\quad 1\end{pmatrix},\\
& G(\ell_1\ 1\ 2)G\begin{pmatrix}\ell_2\quad 4\\ \ell_1-\ell_2\ 3\end{pmatrix},\qquad G\begin{pmatrix}\ell_1\ 1\ 2\\ \ell_2\ 1\ 2\end{pmatrix}G\begin{pmatrix}\ell_2\quad 4\\ \ell_1-\ell_2\ 3\end{pmatrix},\\
& (\ell_1-k_1)^2G\begin{pmatrix}\ell_2\quad 4\\ \ell_1-\ell_2\ 3\end{pmatrix},\qquad G(\ell_1\ \ell_2\ 1\ 2\ 3),
\end{aligned} \tag{A4}$$

while the lone evanescent generator is proportional to the same Gram determinant given in Eq. (A2).

3. Two-loop beetle

As for the other topologies in this appendix, we provide the Gram determinant form of the locally finite ideal for the beetle integral defined in Sec. VII D. A possible choice of basis is

$$\begin{aligned}
\text{rank three:}\ & G\begin{pmatrix}\ell_1\ 1\\ 1\ 2\end{pmatrix}G\begin{pmatrix}\ell_2\ 1\ 2\\ \ell_2\ 3\ 4\end{pmatrix},\qquad G\begin{pmatrix}\ell_1\ 1\\ 1\ 2\end{pmatrix}G\begin{pmatrix}\ell_2\quad 1\quad 4\\ \ell_2-k_1\ 2\ 3\end{pmatrix},\\
& G(\ell_2\ 1\ 2\ 4)G\begin{pmatrix}\ell_1\ 1\\ 1\ 2\end{pmatrix},\qquad G(\ell_2\ 1\ 2\ 4)G\begin{pmatrix}\ell_1\ 1\\ 2\ 3\end{pmatrix},\\
& G\begin{pmatrix}\ell_2\ 1\\ 1\ 2\end{pmatrix}G\begin{pmatrix}\ell_2\ 1\ 2\ 2\\ \ell_1\ 1\ 2\ 3\end{pmatrix},\qquad G\begin{pmatrix}\ell_2\ \ell_1\ 1\ 2\\ \ell_2\ 1\ 2\ 3\end{pmatrix},
\end{aligned}$$

$$
\begin{aligned}
&\text{rank four}: G\begin{pmatrix}\ell_2 & 1\\ 1 & 2\end{pmatrix} G\begin{pmatrix}\ell_1 & 1\\ 2 & 3\end{pmatrix} G\begin{pmatrix}\ell_2 & 1 & 2\\ 1 & 2 & 3\end{pmatrix} G\begin{pmatrix}\ell_2 & 3 & 4\\ 1 & 2 & 3\end{pmatrix},\\
&\quad G\begin{pmatrix}\ell_2 & 1\\ 1 & 2\end{pmatrix} G\begin{pmatrix}\ell_2 & 4\\ 1 & 2\end{pmatrix} G\begin{pmatrix}\ell_1 & 1\\ 2 & 3\end{pmatrix} G\begin{pmatrix}\ell_2-k_1 & 2 & 3\\ 1 & 2 & 3\end{pmatrix},\\
&\quad G\begin{pmatrix}\ell_2 & 1\\ 1 & 2\end{pmatrix} G\begin{pmatrix}\ell_1 & 1\\ 2 & 3\end{pmatrix} G\begin{pmatrix}\ell_2 & 1 & 4\\ \ell_2-k_1 & 2 & 3\end{pmatrix}, \qquad G\begin{pmatrix}\ell_2 & 1\\ 2 & 3\end{pmatrix} G\begin{pmatrix}\ell_2 & 3 & 4\\ 1 & 2 & 3\end{pmatrix} G^2\begin{pmatrix}\ell_2 & 1 & 2\\ 1 & 2 & 3\end{pmatrix},\\
&\quad G\begin{pmatrix}\ell_1 & 1\\ 2 & 3\end{pmatrix} G\begin{pmatrix}\ell_1 & 1 & 2\\ 1 & 2 & 3\end{pmatrix} G\begin{pmatrix}\ell_2 & 1 & 4\\ \ell_2-k_1 & 2 & 3\end{pmatrix}, \qquad G(\ell_2\ 1\ 2\ 3)\, G\begin{pmatrix}\ell_2 & 1 & 2 & 2\\ \ell_1 & 1 & 2 & 3\end{pmatrix}.
\end{aligned}
\tag{A5}
$$

APPENDIX B: RATIONAL COEFFICIENTS OF THE ALL-PLUS AMPLITUDE

In this section we list the rational coefficients for the all-plus gluon amplitude of Eq. (82). In terms of the variable $x = -s_{13}/s_{12}$, we find

$$
\begin{aligned}
\tilde{r}_5^+ &= \frac{1}{x} - \frac{1}{x^2} + \left(\frac{55}{6x^2} - \frac{193}{6x} - \frac{10}{x-1} - 1\right)\epsilon + \left(-\frac{92}{3x^2} + \frac{218}{3x} + \frac{82}{x-1} + \frac{49}{6}\right)\epsilon^2 + \left(\frac{151}{3x^2} - \frac{205}{3x} - \frac{513}{2(x-1)} - 25\right)\epsilon^3,\\
\tilde{r}_6^+ &= -\frac{1}{x^2} + x + \frac{3}{x} - 3 + \left(-10x^3 + 6x^2 + \frac{55}{6x^2} + \frac{191x}{6} - \frac{9}{2x} - \frac{65}{2}\right)\epsilon + \left(82x^3 - \frac{1175x^2}{6} - \frac{92}{3x^2} + \frac{403x}{3} + \frac{50}{x} - \frac{239}{6}\right)\epsilon^2\\
&\quad + \left(-\frac{513x^3}{2} + \frac{1453x^2}{2} + \frac{151}{3x^2} - \frac{4295x}{6} - \frac{133}{x} + \frac{657}{2}\right)\epsilon^3,\\
\tilde{r}_7^+ &= 6 - \frac{6}{x} + \left(3x + \frac{55}{x} - 55\right)\epsilon + \left(-\frac{79x}{2} - \frac{184}{x} + 184\right)\epsilon^2 + \left(\frac{291x}{2} + \frac{302}{x} - 302\right)\epsilon^3,\\
\tilde{r}_8^+ &= -\frac{1}{x^2} + \frac{2}{x} - 1 + \left(\frac{55}{6x^2} - x - \frac{118}{3x} + \frac{247}{6}\right)\epsilon + \left(-\frac{92}{3x^2} + \frac{49x}{6} + \frac{87}{x} - \frac{253}{2}\right)\epsilon^2 + \left(\frac{151}{3x^2} - 25x - \frac{221}{3x} + \frac{1205}{6}\right)\epsilon^3,\\
\tilde{r}_9^+ &= -\frac{1}{x^2} + \frac{2}{x} - 1 + \left(10x^2 + \frac{55}{6x^2} + \frac{8}{3x} - \frac{131}{6}\right)\epsilon + \left(-62x^2 - \frac{92}{3x^2} + \frac{213x}{2} + \frac{107}{3x} - \frac{99}{2}\right)\epsilon^2\\
&\quad + \left(\frac{305x^2}{2} + \frac{151}{3x^2} - 357x - \frac{383}{3x} + \frac{1691}{6}\right)\epsilon^3,\\
\tilde{r}_{10}^+ &= \frac{1}{x^2} - \frac{1}{x} + \left(-\frac{55}{6x^2} + \frac{193}{6x} - \frac{5}{x-1} - 41\right)\epsilon + \left(\frac{92}{3x^2} - \frac{218}{3x} + \frac{11}{x-1} + \frac{767}{6}\right)\epsilon^2 + \left(-\frac{151}{3x^2} + \frac{x}{2} + \frac{231}{4(x-1)} + \frac{205}{3x} - \frac{117}{2}\right)\epsilon^3,\\
\tilde{r}_{11}^+ &= \frac{1}{x^2} - x - \frac{3}{x} + 3 + \left(-5x^3 - 3x^2 - \frac{55}{6x^2} + \frac{43x}{6} + \frac{9}{2x} + \frac{11}{2}\right)\epsilon + \left(11x^3 + \frac{317x^2}{6} + \frac{92}{3x^2} - \frac{382x}{3} - \frac{50}{x} + \frac{497}{6}\right)\epsilon^2\\
&\quad + \left(\frac{231x^3}{4} - \frac{853x^2}{4} - \frac{151}{3x^2} + \frac{3433x}{12} + \frac{133}{x} - \frac{853}{4}\right)\epsilon^3,\\
\tilde{r}_{12}^+ &= \frac{6}{x^2} - \frac{12}{x} + 6 + \left(30x^2 - \frac{55}{x^2} + 21x + \frac{92}{x} - 118\right)\epsilon + \left(-126x^2 + \frac{184}{x^2} - 19x - \frac{221}{x} + 368\right)\epsilon^2\\
&\quad + \left(\frac{51x^2}{2} - \frac{302}{x^2} - 198x + \frac{199}{x} - 182\right)\epsilon^3,\\
\tilde{r}_{13}^+ &= \frac{6}{x} - \frac{6}{x^2} + \left(\frac{55}{x^2} - 30x + \frac{30}{x-1} - \frac{73}{x} + 129\right)\epsilon + \left(-\frac{184}{x^2} + 186x - \frac{126}{x-1} + \frac{331}{x} - 604\right)\epsilon^2\\
&\quad + \left(\frac{302}{x^2} - \frac{915x}{2} + \frac{51}{2(x-1)} - \frac{707}{x} + \frac{1431}{2}\right)\epsilon^3.
\end{aligned}
\tag{B1}
$$

Terms of $\mathcal{O}(\epsilon^4)$ do not contribute to the finite part of the amplitude. The overall coefficient reads

$$C(\epsilon) = \frac{16}{(-3+2\epsilon)^2(-1+2\epsilon)^2(-2+3\epsilon)(-1+3\epsilon)}. \tag{B2}$$

[1] C. G. Bollini and J. J. Giambiagi, Nuovo Cimento B **12**, 20 (1972).
[2] G. 't Hooft and M. J. G. Veltman, Nucl. Phys. **B44**, 189 (1972).
[3] F. V. Tkachov, Phys. Lett. **100B**, 65 (1981).
[4] K. G. Chetyrkin and F. V. Tkachov, Nucl. Phys. **B192**, 159 (1981).
[5] N. Arkani-Hamed, J. L. Bourjaily, F. Cachazo, and J. Trnka, J. High Energy Phys. 06 (2012) 125.
[6] A. V. Kotikov, Theor. Math. Phys. **176**, 913 (2013).
[7] J. M. Henn, Phys. Rev. Lett. **110**, 251601 (2013).
[8] A. V. Kotikov, Phys. Lett. B **254**, 158 (1991).
[9] Z. Bern, L. J. Dixon, and D. A. Kosower, Nucl. Phys. **B412**, 751 (1994).
[10] E. Remiddi, Nuovo Cimento A **110**, 1435 (1997).
[11] T. Gehrmann and E. Remiddi, Nucl. Phys. **B580**, 485 (2000).
[12] J. M. Henn, T. Peraro, M. Stahlhofen, and P. Wasser, Phys. Rev. Lett. **122**, 201602 (2019).
[13] A. von Manteuffel, E. Panzer, and R. M. Schabinger, Phys. Rev. Lett. **124**, 162001 (2020).
[14] M. Bonetti, E. Panzer, V. A. Smirnov, and L. Tancredi, J. High Energy Phys. 11 (2020) 045.
[15] M. Bonetti, E. Panzer, and L. Tancredi, J. High Energy Phys. 06 (2022) 115.
[16] S. Catani, Phys. Lett. B **427**, 161 (1998).
[17] T. Becher and M. Neubert, Phys. Rev. Lett. **102**, 162001 (2009); **111**, 199905(E) (2013).
[18] T. Becher and M. Neubert, J. High Energy Phys. 06 (2009) 081; 11 (2013) 024(E).
[19] E. Gardi and L. Magnea, J. High Energy Phys. 03 (2009) 079.
[20] E. Gardi and L. Magnea, Nuovo Cimento C **32**, 137 (2009).
[21] O. Almelid, C. Duhr, and E. Gardi, Phys. Rev. Lett. **117**, 172002 (2016); N. Agarwal, L. Magnea, C. Signorile-Signorile, and A. Tripathi, Phys. Rep. **994**, 1 (2023).
[22] A. von Manteuffel, E. Panzer, and R. M. Schabinger, J. High Energy Phys. 02 (2015) 120.
[23] A. von Manteuffel, E. Panzer, and R. M. Schabinger, Phys. Rev. D **93**, 125014 (2016).
[24] B. Agarwal, S. P. Jones, and A. von Manteuffel, J. High Energy Phys. 05 (2021) 256.
[25] S. Borowka, N. Greiner, G. Heinrich, S. P. Jones, M. Kerner, J. Schlenk, U. Schubert, and T. Zirke, Phys. Rev. Lett. **117**, 012001 (2016); **117**, 079901(E) (2016).
[26] S. Borowka, N. Greiner, G. Heinrich, S. P. Jones, M. Kerner, J. Schlenk, and T. Zirke, J. High Energy Phys. 10 (2016) 107.
[27] A. von Manteuffel and R. M. Schabinger, J. High Energy Phys. 04 (2017) 129.
[28] L. Chen, G. Heinrich, S. P. Jones, M. Kerner, J. Klappert, and J. Schlenk, J. High Energy Phys. 03 (2021) 125.
[29] C. Anastasiou and G. Sterman, J. High Energy Phys. 07 (2019) 056.
[30] C. Anastasiou and G. Sterman, J. High Energy Phys. 05 (2023) 242.
[31] J. L. Bourjaily, E. Herrmann, and J. Trnka, J. High Energy Phys. 06 (2017) 059.
[32] D. C. Dunbar, J. H. Godwin, G. R. Jehu, and W. B. Perkins, Phys. Rev. D **96**, 116013 (2017).
[33] S. Badger, G. Mogull, and T. Peraro, J. High Energy Phys. 08 (2016) 063.
[34] H. B. Hartanto, S. Badger, C. Brønnum-Hansen, and T. Peraro, J. High Energy Phys. 09 (2019) 119.
[35] E. Panzer, Comput. Phys. Commun. **188**, 148 (2015).
[36] M. Borinsky, H. J. Munch, and F. Tellander, Comput. Phys. Commun. **292**, 108874 (2023).
[37] E. Remiddi and L. Tancredi, Nucl. Phys. **B880**, 343 (2014).
[38] C. Duhr, A. Klemm, C. Nega, and L. Tancredi, J. High Energy Phys. 02 (2023) 228.
[39] F. J. Dyson, Phys. Rev. **75**, 1736 (1949).
[40] S. Weinberg, Phys. Rev. **118**, 838 (1960).
[41] L. D. Landau, Nucl. Phys. **13**, 181 (1959); J. D. Bjorken, Experimental tests of quantum electrodynamics and spectral representations of Green's functions in perturbation theory, Ph.D. thesis, Stanford University, 1959; N. Nakanishi, Prog. Theor. Phys. **22**, 128 (1959).
[42] S. Mizera and S. Telen, J. High Energy Phys. 08 (2022) 200.
[43] H. S. Hannesdottir, A. J. McLeod, M. D. Schwartz, and C. Vergu, Phys. Rev. D **105**, L061701 (2022).
[44] E. Gardi, F. Herzog, S. Jones, Y. Ma, and J. Schlenk, J. High Energy Phys. 07 (2023) 197.
[45] Y. Hahn and W. Zimmermann, Commun. Math. Phys. **10**, 330 (1968); W. Zimmermann, Commun. Math. Phys. **11**, 1 (1968).
[46] N. Nakanishi, Prog. Theor. Phys. **17**, 401 (1957); *Graph Theory and Feynman Integrals* (Gordon and Breach, New York, 1971).
[47] S. Mizera, Phys. Rev. D **104**, 045003 (2021).
[48] G. F. Sterman, *An Introduction to Quantum Field Theory* (Cambridge University Press, Cambridge, England, 1993), 10.1017/CBO9780511622618; J. Collins, *Foundations of Perturbative QCD* (Cambridge University Press, Cambridge, England, 2013), Vol. 32, 10.1017/CBO9780511975592.

[49] R. J. Eden, P. V. Landshoff, D. I. Olive, and J. C. Polkinghorne, *The Analytic S-Matrix* (Cambridge University Press, Cambridge, England, 1966).
[50] S. Weinzierl, *Feynman Integrals* (Springer, Cham, 2022), 10.1007/978-3-030-99558-4.
[51] G. F. Sterman, Phys. Rev. D **17**, 2773 (1978); S. B. Libby and G. F. Sterman, Phys. Rev. D **18**, 3252 (1978); Phys. Rev. D **18**, 4737 (1978).
[52] T. Peraro, J. High Energy Phys. 07 (2019) 031.
[53] Z. Bern, L. J. Dixon, and D. A. Kosower, J. High Energy Phys. 01 (2000) 027.
[54] Z. Bern, A. De Freitas, and L. J. Dixon, J. High Energy Phys. 09 (2001) 037.
[55] E. W. N. Glover, C. Oleari, and M. E. Tejeda-Yeomans, Nucl. Phys. **B605**, 467 (2001).
[56] S. Caron-Huot and K. J. Larsen, J. High Energy Phys. 10 (2012) 026.